Evolution and Characterization of Partially Stabilized Zirconia (7wt% Y_2O_3) Thermal Barrier Coatings Deposited by Electron Beam Physical Vapor Deposition

by

Jeremy Bernier

A Master's Thesis

Submitted to the Faculty

of the

WORCESTER POLYTECHNIC INSTITUTE

in partial fulfillment of the requirements for the

Degree of Master's of Science

in

Materials Science and Engineering

by

_____

May 18, 2001

APPROVED:

_____

Richard D. Sisson Jr., Advisor
Materials Science and Engineering Program Head
Mechanical Engineering Department

Abstract

Thermal barrier coatings (TBCs) of ZrO_2-7wt% Y_2O_3 were deposited by electron beam physical vapor deposition (EB-PVD) onto stationary flat plates and cylindrical surfaces in a multiple ingot coater. Crystallographic texture, microstructure, and deposition rate were investigated in this thesis. The crystallographic texture of EB-PVD TBCs deposited on stationary flat surfaces has been experimentally determined by comparing pole figure analysis data with actual column growth angle data. It was found that the TBC coating deposited directly above an ingot exhibits <220> single crystal type crystallographic texture. Coatings deposited between and off the centerline of the ingots the exhibited a <311>-type single crystal texture. For coatings deposited in the far corners of the coating chamber either a <111> fiber texture or a <311> single crystal type texture existed. The crystallographic texture of EB-PVD TBCs deposited on cylindrical surfaces was characterized using x-ray diffraction (XRD) at different angular positions on the cylinder substrate. XRD results revealed that crystallographic texture changes with angular position. Changes in crystallographic texture are attributed to the growth direction of the columns and substrate temperature. Growth direction is controlled by the direction of the incoming vapor flux (i.e. vapor incidence angle), in which competition occurs between crystallites growing at different rates. The fastest growing orientation takes over and dominates the texture. Substrate temperature variations throughout the coating chamber resulted in different growth rates and morphology.

Morphology differences existed between cylindrical and flat plate surfaces. Flat cross sectional surfaces of the coatings exhibited a dense columnar structure in which the columns grew towards the closest vapor source. Surface features were found to be larger

for coatings deposited directly above an ingot than coatings deposited away from the ingots. Morphological differences result from substrate temperature changes within the coating chamber, which influences growth kinetics of the coating. Cylindrical surfaces revealed a columnar structure in which columns grew towards the closest vapor. Porosity of the coating was found to increase when the angular position changed from the bottom of the cylinder. Change in angular position also caused the column diameter to decreases. Morphology changes are attributed to self-shadow effects caused by the surface curvature of the cylinder and vapor incidence angle changes. Overall, the microstructure and crystallographic texture of EB-PVD coatings was found to depend on the position in the coating chamber which was found to influence substrate temperature, growth directions, and shadowing effects.

The coating thickness profiles for EB-PVD TBCs deposited on stationary cylinders have been experimentally measured and theoretically modeled using Knudsen's cosine law of emissions. A comparison of the experimental results with the model reveals that the model must to be modified to account for the sticking coefficient as well as a ricochet factor. These results are also discussed in terms of the effects of substrate temperature on the sticking coefficient, the ricochet factor, and coating density.

Acknowledgements

I would like to thank my advisor, Professor Richard D. Sisson Jr, for his encouragement, support, advice and overall guidance during this thesis. Without his motivation and knowledge I would not be writing this part right now. I would also like to thank him for all the good times and memories that I have while being his student. I would like to thank Dr. Sudha Bose and Greg Levan of Pratt & Whitney for all the help and support they have given me in order to complete this project. They have aided in my education tremendously. Further thanks goes to Md. Maniruzzaman and Bill Weir for their time and help they have given me.

May 18, 2002

Jeremy Bernier

Table of Contents

List of Figures

List of Tables

1. Introduction

Thermal Barrier Coatings (TBCs) are currently used on high-pressure high-temperature turbine blades to increase efficiency in aerospace and land based gas engines. TBCs are typically comprised of an insulating ceramic coating that reduces metal temperature and a bond coat, which allows for better adhesion of the TBC to the superalloy substrate [1]. The ceramic coating properties required for turbine engine applications are achieved through the selection of material properties and coating process parameters. Desired ceramic properties include: low thermal conductivity, a relatively high coefficient of thermal expansion, thermodynamic stability in the gas turbine environment, and mechanical stability during thermal cycling [2].

The development of TBCs has focused on zirconia-yttria ceramics [3]. Such coatings can reduce the metal temperature of an air-cooled turbine blade by 50°-200°C [3]. Zirconia partially stabilized with 7% Yttria (YPSZ) has demonstrated its capabilities as the most durable material for TBCs on turbine blades sthus far. It consists of non-transformable tetragonal t' phase with a c/a ratio close to unity [4].

Currently, the YPSZ TBCs are applied to turbine blades by two methods, one known as Electron Beam Physical Vapor Deposition (EB-PVD) and the other method known as Plasma Spraying (PS) [4]. EB-PVD processed TBCs offer significant benefits over PS TBCs because of their columnar microstructure. The columnar microstructure provides outstanding resistance against thermal shock and mechanical strains, which are associated with high temperature high-pressure turbine blades. PS coatings exhibit a laminar structure that consists of splats with cracks parallel to the surface structure which effects cyclic life of the TBC [5].

During the EB-PVD coating process, the part to be coated is suspended in a vacuum chamber over a solid YPSZ vapor source or ingot heated by an electron beam gun. The coating vapors diffuse throughout the vacuum chamber and condense on the part, thus forming the desired YPSZ TBC. There are several process parameters that have an effect on the outcome of the coating thickness and microstructure. Such process parameters include deposition rate, substrate temperature, distance height, and chamber pressure [6].

Research Objective

The principle objective of this research is to determine how the position in a multiple ingot EB-PVD coater affects the microstructure and crystallographic texture of TBCs deposited onto stationary geometrical surfaces. This research also compares how well a theoretical coating thickness model compares with experimental results and discusses possible reasons for disagreement. The work performed in this thesis includes:

1. Microstructural Characterization of EB-PVD TBCs deposited on flat plates and cylindrical surfaces at various locations and positions in the coating chamber.
2. Characterization of crystallographic texture on flat plates and cylindrical surfaces at various locations and positions within the coating chamber.
3. Calculating growth angles associated with TBC columnar structure in order to understand how column growth angles, vapor incidence angles, and pole figure analysis angles are related to crystallographic texture and a primary growth plane.
4. Evaluated how coating density and coating thickness changed with respect to location and angular position within the coating chamber on cylindrical surfaces.

5. Compared WPI's TBC thickness prediction model to the measured TBC thickness values on cylindrical surfaces in order to evaluate the validity of the model.

Thesis Organization

The thesis is divided into five chapters. Chapter I presents the introduction that provides an overview of thermal barrier coatings and the research that was conducted during this project. Chapter II presents a review of the relevant literature. The literature review focuses on thermal barrier coatings in general and the process by which they are applied to a turbine blade. It also focuses on the microstructure and crystallographic texture of TBCs and the process parameters that influence them. The literature also contains information on a theoretical coating thickness prediction model. Chapter III presents a series of three articles that describe the various aspects of this research. Article I, titled **"***Deposition Rates of EB-PVD TBCs on Cylindrical Surfaces*" describes how well the theoretical coating thickness model agrees with the experimental determined results. Possible explanations are given to explain any differences. Article II, titled **"***Microstructural Evolution of EB-PVD TBCs on Cylindrical Surfaces*" describes how microstructure and crystallographic texture vary as a function of position on a cylinder surface. It also describes how density changes as a function of angular position on a cylinder. Both articles I and II were presented at the 26th Annual International Conference on Advanced Ceramics and Composites, Jan. 13-18, 2002 Cocoa Beach, FL and have been accepted for publication in the *Ceramic Engineering and Science Proceedings*. Article III, titled "*Crystallographic Texture and Column Growth Direction of EB-PVD TBCs Deposited on Flat Surfaces in a Multiple Ingot Coating Chamber* " describes

crystallographic texture type with respect to chamber position on flat surfaces and x-ray diffraction texture characterization. Article III was submitted to Acta Materialia May 18, 2002. Chapter IV is a summary of all the results of the three papers. Chapter V is a recommendation section for future work that should be conducted on TBCs to better understand the microstructure and texture associated with a turbine blade.

Chapter II

Thermal Barrier Coatings and the EB-PVD Process-A Review

2. Literature Review

2.1 Thermal Barrier Coatings (TBCs)

The concept of a ceramic TBC is to provide insulation to critical air-cooled metal components such as turbine blades. An important application is in turbine engines where there are several ways to take advantage of ceramic insulation at high temperatures. Such advantages are an increased engine reliability by reducing the metal substrate temperature by 50°C to 220°C, increased engine efficiency and power by maintaining current metal temperatures and increasing gas temperature, and reduce fabrication cost by eliminating elaborate cooling schemes [2]. A diagram of a duplex TBC system is presented in Figure 1. The temperature gradient across the TBC system is influenced by the thermal conductivity and the thickness of the ceramic coating, as well as the cooling airflow rate [2,7].

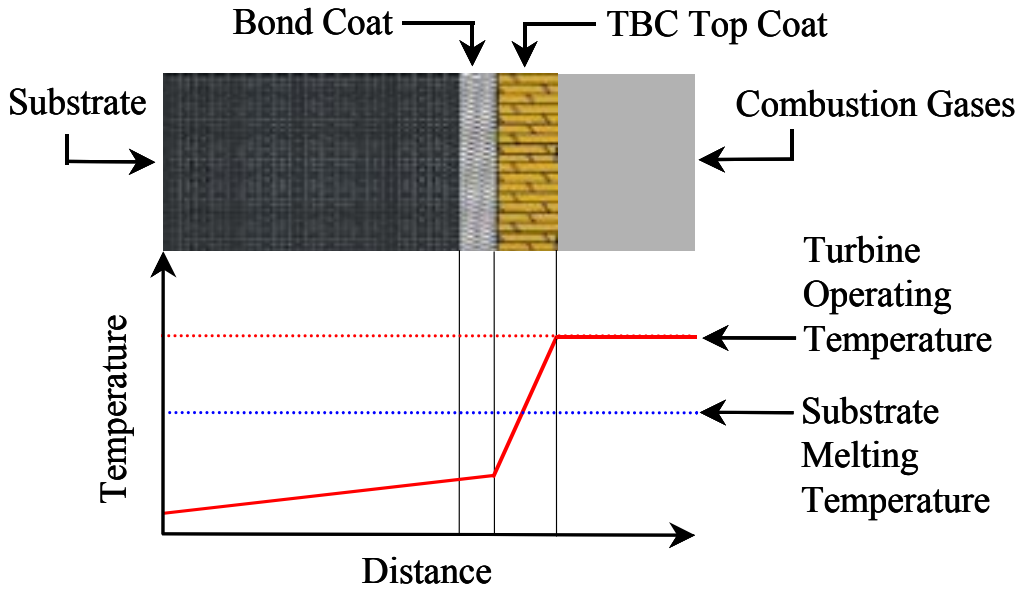

Figure 1: TBC profile and temperature gradient [8]

A duplex system refers to the bond coat and TBC itself. Bond coats are applied to reduce the difference between the thermo-mechanical properties of the ceramic coating layer and the substrate. The function of the bond coat is also to provide oxidation resistance for the substrate material and to provide good coating durability during thermal cycling conditions [9, 10]. Experimental studies have demonstrated that composition, microstructure, and thickness of the bond coat influence the overall performance and durability of the duplex TBC system [11,12].

Aluminized and MCrAlY bond coats are the two generally accepted bond coats used in today's industry [13]. The M stands for either Nickel or Cobalt. In MCrAlY bond coats, the percentage of the elements present (composition) effects the TBC performance. They are applied by such processing techniques as plasma spraying (PS) or physical vapor deposition (PVD). Aluminized bond coats are produced by pack -aluminizing either the already applied bond coat (by PS or PVD) or the substrate material itself. The substrate material is usually a superalloy when referring to turbine engines. The resulting bond coat layer exhibits good oxidation resistance by forming a protective Al_2O_3 oxide layer upon high temperature exposure. Diffusion aluminided bond coats are a recent development that are produced by pack-cementization [13].

When selecting a ceramic material to be used for a TBC in high-pressure high temperature environments, many material properties must be considered. Such considerations include a high thermal expansion coefficient, low thermal conductivity, chemical stability in the oxidizing gas turbine environment, and high thermal shock resistance during thermal cycling [2,12,14,15]. The most durable TBC are those formed from compositions taken from the two-phase (partially stabilized) region of the zirconia-

yttria equilibrium phase diagram [3]. Particularly compositions of zirconia with 6-8% yttria seem to be the "most state of the art" TBC available for turbine engine operating conditions [4].

The Zirconia-Yttria phase diagram presented in Figure 2, predicts a phase separation during cooling into a high yttria cubic (fluorite) phase, F, and a low yttria tetragonal phase, T, for cooling between 2300° and 600°C. With further cooling to room temperature this equilibrium low yttria tetragonal phase is expected to transform martensitically to a monoclinic structure. This is due to lower free energy at lower temperatures. Under certain conditions the tetragonal phase may be retained metastably at room temperatures.

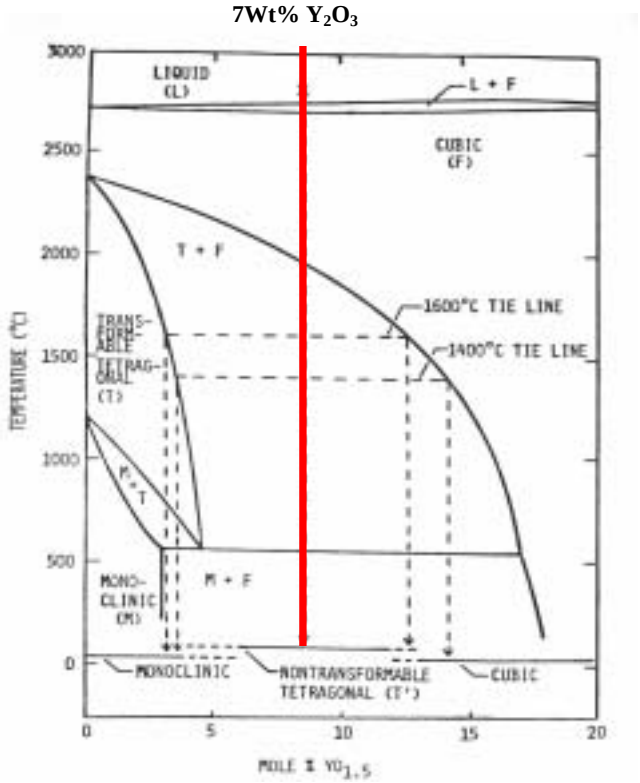

Figure 2: Equilibrium Zirconia-Yttria Phase Diagram [Ref 18] Horizontal Bars Indicate Phases Observed on Quenching. Dashed Lines Indicate tie Lines and Compositions Lines for Quenched Phases

In physical vapor deposition coatings, the main phase observed at room temperature is a non-equilibrium, high ytrria tetragonal phase, known as T' as shown in Figure 3[16,17]. This phase differs from the metastable low yttria tetragonal phase because it is stable with respect to the monoclinic transformation. T' forms because the quenching process prevents compositional adjustments required for the development of equilibrium amounts of low-yttria tetragonal and high yttria cubic phases [3]. The transformation from high yttria cubic phase to T' is a diffusionless phase transforming [3,18]. The T' phase is believed to decompose rather slowly to the equilibrium tetragonal and cubic phase during high temperature exposure [3,18]. T' is unstable with respect to diffusion at high temperatures; therefore additional phase separation into the equilibrium high yttria cubic and low yttria tetragonal phases can be expected. During cooling, the polymorphic transformation from a tetragonal (high temperature, low Yttria) structure to the low temperature monoclinic structure is accompanied by an increase volume change (3-5%) [19]. The stresses associated with this volume change are detrimental to TBC coatings because of spallation [3]. The structural changes can be visually seen in Figure 3. Notice the lattice shifts and the height of the crystal changes and also the density increases going from monoclinic to tetragonal.

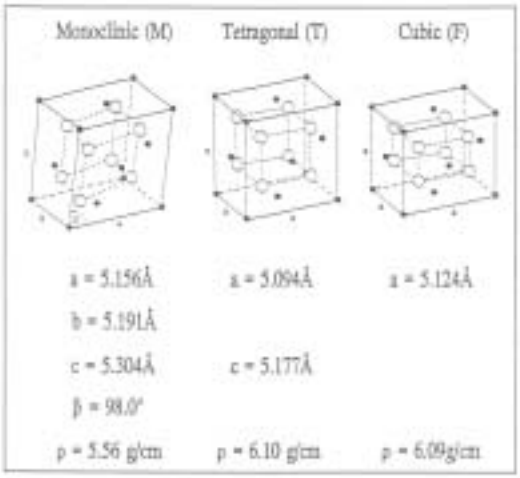

Figure 3: Phase Transformation Structures of YPSZ [13]

Two ways of applying a TBC to a turbine blade are by plasma spray (PS) and electron beam physical vapor deposition (EB-PVD) [2,4,9,13,15,16,17]. Plasma sprayed partially stabilized zirconia (PSZ) coatings have a rough coating surface and relatively large porosity between the splat quenched grains. The porosity has been proven to increase the thermal shock resistance of PSZ coatings [5,7, 13]. The interface between the bond coat and the PSZ coating is rough, which enhances the mechanical and structural properties of the coating. EB-PVD coatings exhibit strain-tolerant and textured columnar grain structures with smooth coating surface and TBC/ bond coat interface [5]. EB-PVD coatings have demonstrated a superior durability at high temperature cyclic oxidation and flight service environments due to strain tolerances [7]. In both PS and EB-PVD there are many critical processing parameters that must be considered in order to produce constituent and optimal TBCs. In the work presented in this thesis, the EB-PVD process was used to apply the TBC of Yrttria Partially Stabilized Zirconia.

2.2 Electron Beam Physical Vapor Deposition (EB-PVD)

EB-PVD is an evaporation process for applying ceramic thermal barrier coatings to gas turbine engine parts [10]. It has been the favored deposition process technique for TBCs because of the increased durability of coating that is produced when compared to other deposition processes. EB-PVD TBCs exhibit a columnar microstructure that provides outstanding resistance against thermal shocks and mechanical strains [4]. Figure 4 presents a diagram of the coating chamber where the EB-PVD process takes place.

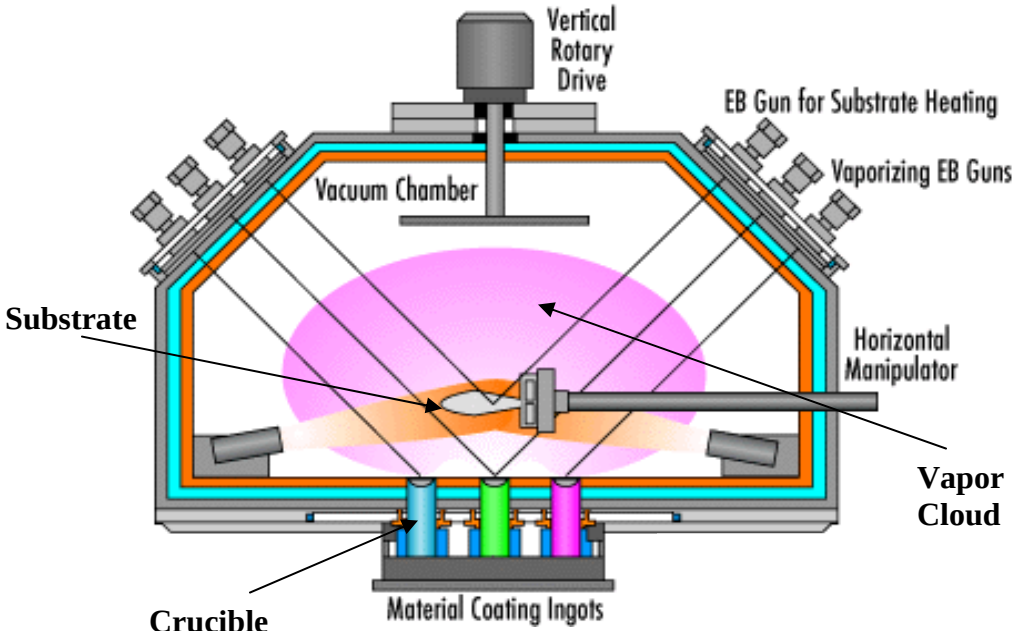

Figure 4: EB-PVD Coating Chamber [20]

The EB-PVD process (Figure 4) takes place in a vacuum chamber consisting of a vacuum-pumping system, horizontal manipulator, a water-cooled crucible containing a ceramic ingot to be evaporated, an electron-beam gun, and the work piece being coated [21]. The electron beam gun produces electrons, which directly impinge on the top surface on the ceramic coating, located in the crucible, and bring the surface to a

temperature high enough that vapor steam is produced. The vapor steam produces a vapor cloud, which condenses on the substrate and thus forms a coating. The substrate is held in the middle of vapor cloud by a horizontal manipulator that allows for height variation in the chamber. During the coating process, oxygen or other gases may be bled into the vapor cloud in order to promote a stoichiometric reaction of ceramic material. An "over source" heater or an electron beam gun may be used for substrate heating, which keeps the substrate at a desired temperature.

The primary control variables for the coating process are the ingot feed rate, ingot size, gun current, and over source heater power [10]. The feed rate and size controls how much mass is to be evaporated by the gun current. The gun current controls how much power is transmitted to the melt pool, and thus controls melt pool temperature for the evaporation rate and deposition rate. The maximum gun current is limited by the stability of the ingot melt surface. Too high a current overheats the ingot surface causing spattering, thus loosing mass evaporated. The melt pool is a major source of heat energy for the substrate as well as substrate heating if used. The substrate temperature is important because it controls many of the deposited coatings material properties.

A source of substrate heating that is uncontrollable is the time in the coater. As parts are coated, ceramic coating builds up on the chamber walls changing the heat dynamics of the chamber, thus effecting substrate temperature. Therefore, chamber temperature varies depending on when the coating chamber was last cleaned. Overall, substrate temperature is hard to control in the coating process [10].

The coating operator must control the primary variables involved in the coating process, as well as beam sweep frequency and rotation rate, which are set prior to the

coating process. Beam sweep frequency refers to the irregular scanning pattern the electron beam gun makes on the ingot surface.

2.3 Coating Thickness Prediction Model

The Knudsen Cosine Law was developed into a coating thickness prediction equation for a variety of receiving surfaces in an EB-PVD coater [21]. The model predicts coating thicknesses at varying distance and angles in a PVD coater, as seen in Figure 5.

The TBC thickness predictions were calculated using a Visual Basic program and the Knudsen's cosine law of emissions which states [21]:

$$d = \left[\frac{M_e}{\rho_{coating}} \left(\frac{\cos\theta \cdot \cos\phi}{\pi \cdot r^2} \right) \right]$$

d = Coating Thickness(m)
M_e = Mass of the ingot evaporated (0.35kg)
$\rho_{coating}$ = Density of coating (6050 kg/m^3) (Ref 6&8)
r = Radial distance from emitted to received surfaces(m)
θ = Angle between the radial distance and received surface normal (degrees)
ϕ= Angle between the radial distance and emitted surface normal (degrees)

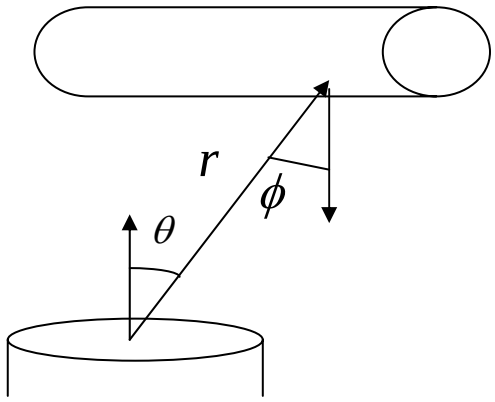

Figure 5: Prediction Model for TBC Deposited on a Cylinder[6,33]

The mass evaporated is the cross section area of the ingot times the length evaporated divided by the density of the ingot. The Visual Basic program integrates over the cross section area of the ingot to a point of the cylinder surface. By doing so, it calculates all possible combinations of θ and ϕ. The program then repeats the process by selecting a different point position of a cylinder. The program also takes into consideration the height on the cylinder above the ingot surface through a radial distance.

2.4 Microstructure

Thorton described the condensation of evaporated molecules as a three-step process [22]. First, incident atoms transfer kinetic energy to the lattice and become loosely bonded "adatoms". These "adatoms" then diffuse over the surface, exchanging energy with the lattice and other absorbed species, until they either are desorbed by evaporation or become trapped at the lowest-energy lattice sites. Finally, the incorporated "adatoms" readjust their position within the lattice by bulk diffusion processes. Depending upon the deposition materials and processing parameters, the characteristics of surface and bulk diffusion during condensation vary significantly, resulting in various microstructures and coating properties [22]. Process parameters refer to such variables as the chamber pressure, substrate temperature, electron beam current, and deposition rate which is controlled by the melt pool temperature, substrate rotation, and substrate height [23].

EB-PVD coatings are also affected by the self-shadowing, which affects microstructure and coating thickness. Self-shadowing refers to the simple geometric interaction between the roughness of the growing surface and the angular directions of the arriving molecules [22]. Assuming a point-evaporation-source and a point-substrate, the thickness of the resulting TBC coating, T_c, is dependent on the weight of the material evaporated (w), the density of the material (ρ), and the distance from the point-evaporation-source to the substrate, Z [24]. On plane-surface substrates with a point source, the equation becomes:

$$Tp = \frac{w\cos\theta}{4\pi\rho Z^2} = Tc\left(\frac{Zo}{Z}\right)^3$$

Where Tp is the coating thickness at point P, Zo is the shortest distance from the plane to the source, and θ is the inclination of the substrate at P to the molecular rays emitted by the vapor source that impinge the substrate at point P. Since EB-PVD process mostly uses circular shaped ingots as the vapor source, integrating over the circular surface from 0 to 2π gives the coating thickness (Tp) the expression:

$$Tp = \frac{w}{8\pi^2 \rho} \int \frac{d\theta}{z^3}$$

Zone models have been constructed through previous studies of TBCs and are presented in Figure 6 [22,13].

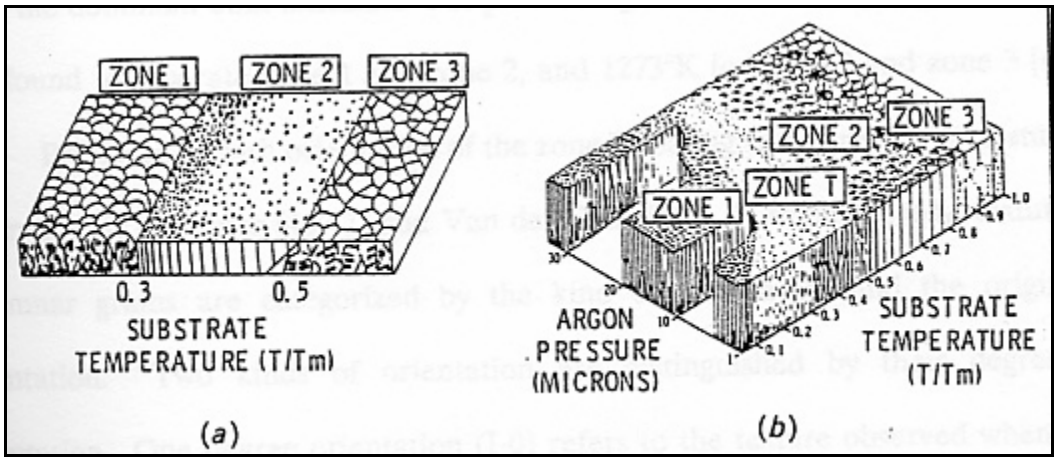

Figure 6: Structural zone models for coating growth. (a) Movchan & Demchishin[25] (b) Thorton[22]

Zone 1 (Tsub / Tmp<.3) consists of dome dome-toped, tapered crystals separated by voided boundaries [22,25]. The internal structure of the crystals is poorly defined, with a high dislocation density. Zone 1 features are believed to be a result of the dominant shadowing effect and insufficient surface diffusion of the adatoms. Substrate surface roughness is complementary in producing shadow induced Zone 1 boundaries, which makes it difficult to achieve uniform dense coatings deposited on complex shaped substrates. A transition zone between zone1 and zone 2 (ZoneT) has been added to

include the infinite smooth surface of zone 1,i.e no surface diffusion and no shadowing [22]. Zone 2 (.3<Tsub/Tmp.5) consists of dense columnar grains with smooth, sometimes faceted surfaces, resulting from surface diffusion dominant condensation. Movchan & Demchishin [25] also suggest that the grains grow by surface recrystallization. Preferred growth orientation of the columnar grains has been observed in zone 2 as seen in Figure 6. Zone 3 (.5<Tsub/Tmp<1) consists of equiaxed grains with a bright surface. The grain diameters increase with Tsub/Tmp and yield an activation energy that corresponds to bulk diffusion [22].

Although EB-PVD PSZ coatings have exhibited exceptional performance and durability as TBCs, processing/structure/ properties relationship study should provide a better understanding of the process of condensation and the failure of TBCs, and should lead to an optimization of TBCs[13]. As previously described, EB-PVD coatings exhibit processing dependent characteristics such as zone structures, defect microstructures, and crystallographic texture due to anisotropy. This anisotropy leads to mechanical and thermal property differences [13].

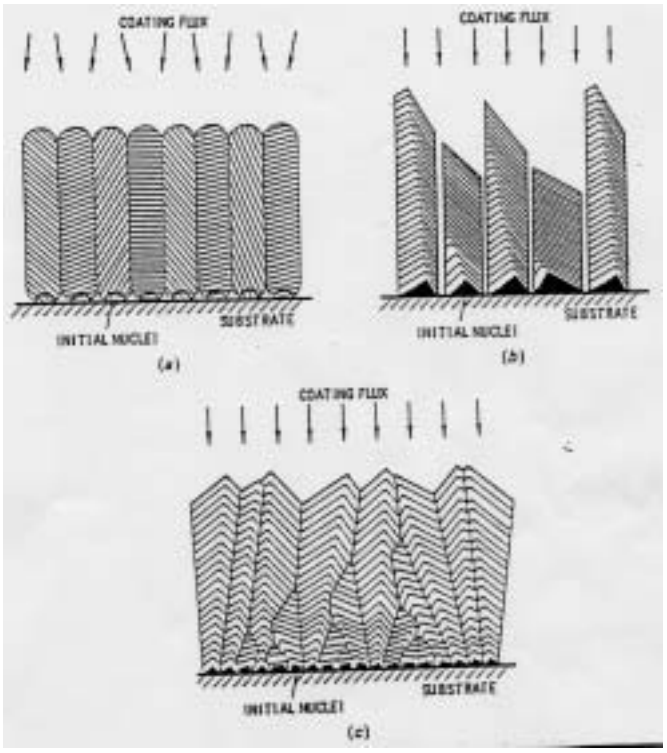

Figure 7: Extreme Growth Structures in Zone 2 which Show Preferred Growth Orientation [22]. a) No Surface Diffusion and Unity Condensation Coefficient, b) No Surface Diffusion & Crystallographic Dependent Condensation Coefficient, c) Infinite Surface Diffusion.

2.5 Crystallographic Texture

When YPSZ is deposited by EB-PVD onto stationary or rotated substrates, many different crystallographic textures are found as presented in Table 1.

Table 1: Textures Present from Previous Reports in Literature[Ref below] (HPTB= High Pressure Turbine Blade)

Reference	Texture	Substrate geometry	Stationary/Rotated
26	{100},{113}	flat plates	rotated
30	{220}, {200},	flat plates	stationary
27	{111}, {311}, {422}	flat plates	stationary
27	{200}, {220},{311}	HPTB	rotated
28	{111}, {113}, {110}	-	stationary
28	{100}	-	rotated
29	{101}	flat plates	stationary
16	{311}	flat plates	stationary

Texture is dependent upon many variables that include surface energy, surface and volume diffusion, coating composition, and depositions conditions that include chamber pressure and substrate temperature, as well as how texture is defined [26]. Many reports in literature have found that substrate temperature influences crystallographic orientation [26,27,28,]. At elevated substrate temperatures, there is greater mobility of the condensing coating molecules. This causes the molecules to move into a more stable or lowest energy configurations that result in a higher degree of ordering in the lattice causing crystallographic orientation [26,29]. Schultz, Oettel and Bunk [26] found that the one preferred orientation during film growth is the vapor incidence angle (VIA). This angle is defined as the angle between the coating vapor flux and the substrate surface normal. The VIA was also found to influence crystallographic texture by many other authors as well [26,27,28,29]. Overall, texture is more sensitive to the VIA and deposition conditions for stationary substrates than rotated substrates as indicated by Schultz and Schmucker [4]. The periodic bond chain theory [26,28] states that the {111}, {100}, {110}, and {113} as the predominant growth directions for stationary substrates. However, no strong growth direction was favored as the preferred growth direction. If the substrate was rotated, the rotation strictly controls the texture and columnar morphology.

Sohn, Biederman, and Sisson [27] have stated that crystallographic orientation may be affected by changes in both the VIA and the deposition parameters. The VIA can be varied by substrate position in the coating chamber and substrate geometry. Columns grow toward the vapor source at a certain angle. The columns have certain planes normal to the column axis, but different planes result since they are parallel to the substrate

surface as shown in Figure 8. In other words, texture patterns may be taken normal to the surface but that may not be normal to the columnar growth direction since columns grow towards the vapor source [30].

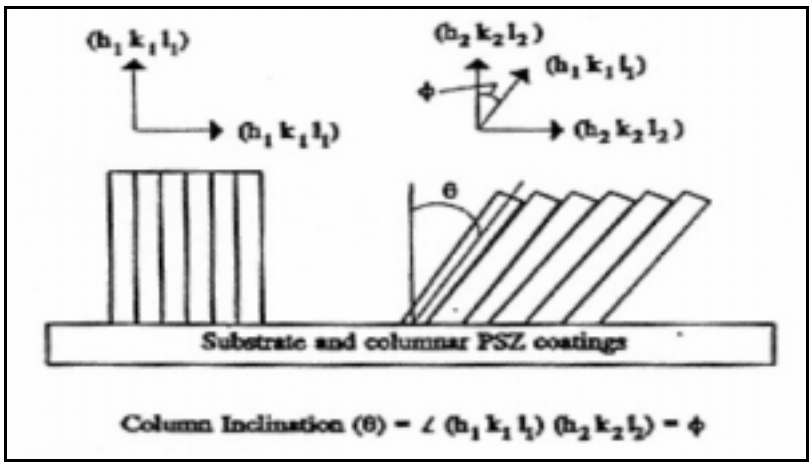

Figure 8- Effects of Vapor Incidence Angle [13]

Schultz, Oettel and Bunk [26] also mention that texture may be influenced by high super saturation due to high growth rates. This may favor dendritic directions in the lattice rather than low energy equilibrium planes during film growth. Additionally, a "feathery like" structure has been found within each columnar structure of the TBC. The growth direction of the "feathery structure arms" may differ from the overall column axis [26,28,29].

Preferred growth orientation or texture of zone 2 (Figure6) coating structures has been studied and modeled by Bauer[31] and Van der Drift [32]. In Bauer's study, textures of columnar grains were characterized by the kind of orientation and origin of the orientation. The two kinds of orientation are distinguished by their degree or orientation. One degree orientation (I-0) refers to texture observed when one crystallographic axis of the crystals points in one preferred direction. Two-degree orientation (II-0) results when two crystallographic axes point in the same direction. The limiting case for two-degree

orientation is single crystal type texture in which all crystals are oriented in the same direction. Bauer also categorized the origin of texture by nucleation, growth, and nucleation-growth. Nucleation orientation results from nucleation with a preferred plane parallel to the local substrate surface when the vapor is supersaturated and the nucleation rate is high. However, nucleation orientation appears only as an initial orientation. Growth orientation develops in a supersaturated region in which two-dimensional nucleation on the growing crystal surface is no longer a rate determining step and in which three dimensional nucleation of randomly oriented crystals remain sufficiently infrequently. In this case, growth competition between differently oriented crystals takes place. Thus, growth orientation results from the difference in the number of vapor flux particles condensing on the individual crystals (growth rate). The difference in the growth rate depends on the planes that form the crystal surface and the orientation of the planes relative to the vapor flux. Growth orientations are generally the final orientations. In general Bauer concluded that the surviving crystals and orientation might be a result of crystals that receive the greatest vapor flux [31].

Van der Drift observed the increase in the orientation sharpness during the vertical growth of the coatings and concluded that crystallographic texture is a result of a *process of evolutionary selection* of favorable orientations [32]. This states the crystals with the highest component of growth rate, perpendicular to the substrate, are selected and the texture is amplified as the thickness of the coating increases [32]. The vertical growth rate was considered a function of crystal orientation and the angle of incidence to the substrate [32].

The technical importance of texture investigations comes from the anisotropy of the elastic moduli and coefficient of thermal expansion (CTE) with the T' phase of YPSZ. It has shown that for up to 8% Y2O3 in ZrO_2 the CTE of the c axis is greater than the a axis [13] and the Young Modulus is two times higher in the {100}-growth direction compared to the {111}-growth direction [13]. With TBCs having different crystallographic orientations, texture investigation offers a potential to further increase the lifetime of the coating due to lower mechanical stresses.

References

1. Schultz, U., Fritscher, K., Leyens, C. "Two-Source Jumping Beam Evaporation for Advanced EB-PVD TBC Systems" *Surface and Coatings Technology* 133-134 (2000) p.40-48.

2. Bratton, R.J., and Lau, S.K. "Zirconia Thermal Barrier Coatings" *Science and Technology of Zirconia* 1980 p. 226-240.

3. Miller, R.A., Smialek, J.L., and Garlick, R.G. "Phase Stability in Plasma Sprayed Partially Stabilized Zirconia-Yttria" *Advances in Ceramics: Science and Technology of Zirconia* vol.3 (1981) p.241-253.

4. Schultz,U., Fritscher, K., Ratzer-Scheibe, H.J., Kaysser, W.A. and Peters, M. "Thermocyclic Behavior Of Microstructurally Modified EB-PVD Thermal Barrier Coatings" *Materials Science Forum* vols. 251-254 (1997) P.957-964.

5. Beele, W., Marijnissen, A. and Van Lieshout, A. " The Evolution of Thermal Barrier Coatings -status and upcoming solutions for todays key issues" *Surface and Coatings Technology* 120-121 (1999) p.61-67.

6. Weir, W.C.S., Sisson R.D. Jr, Bose, S., "Rule-Based software tool to specify the manufacturing process parameters for a contoured EB-PVD coating," *Intelligent Systems in Design and Manufacturing III, Bhaskaran Gopalakrishnan, Angappa Gunasekaren, Editors, Proceedings of SPIE* Vol 4192 (2000)©@ 2000 SPIE 0277-786X/00/$1500, p 330-337.

7. Miller, R.A. "Current Status of Thermal Barrier Coatings- An overview" *Surface and Coatings Technology*, vol.30 (1987) p. 1-11.

8. Ballard, J.A. " Phase Transitions in thermal Barrier Coatings" *RPI Materials Science Dept* http://www.rpi.edu/dept/materials/surp/ballard.ppt 2000

9. Bennett, A., "Properties of Thermal Barrier Coatings" *Material Science and Technology* vol.2 1986 p.257-261.

10. "Vapor Phase Intelligent Processing of Thermal Barrier Coatings" *IPM-PVD DARPA* May 31, 2000

11. Wortman, D.J., Duderstadt, E.C. and Nelson, W.A., "Bond Coat Development for Thermal Barrier Coatings" *Journal of Engineering for Gas Turbines and Power*, vol.112 (1990) p.527-530.

12. Wortman, D.J., Nagaraj, B.A., and Duderstadt, E.C., "Thermal Barrier Coatings for Gas Turbine Use" *Materials Science and Engineering* vol.A121 (1989) p. 433-440.

13. Sohn, Y.H., "Thermal Barrier Coatings," *Characterization and Life Prediction of Vapor Deposited Partially Stabilized Zirconia Thermal Barrier Coatings*, Worcester Polytechnic Institute Worcester, MA (1993) p.4-33.

14. Colwell,J.A., "Thermal Barrier Coatings for Engine Applications" Report by Metals and Ceramic Information Center vol. MCIC-86-C2 (1986).

15. Lee. E.Y., "Phase transformations in PSZ," *Life Prediction and Failure Mechanisms for Thermal Barrier Coatings*, Ph.D Dssertation Worcester Polytechnic Institute Worcester, MA (1993) p.8-19

16. Lelait, L., Alperine, S. and Diot, C. "Microstructural Investigation of EB-PVD Thermal Barrier Coatings" *J. de Physique IV, Colloque* C9, 3(1993) p. 645-654.

17. Schutz, U., Fritscher, K. Peters, M. Leyens, C. "High Temperature Aging of EB-PVD Thermal Barrier Coatings" *DLR-German Aerospace Center-Institute of Materials Research*, Cologne Germany

18. Scott, H.G. "Phase Relationships in the Zirconia Yttria System" *Journal of Material Science*, vol.10 (1975) p.1527-1535.

19. Stevens, R, *Introduction to Zirconia* Magnesium Elecktron Ltd, New York, 2000

20. Pennsylvania State University, Applied Research Laboratory, High Energy Processing Laboratory, EB-PVD picture[schematic.gif]. Availible from: http://www.arl.psu.edu/areas/ebpvd/ebpvd.html. Last Accessed 2000 July 11.

21. Weir, W.C.S., " Development of a rule based software system for the fabrication of a contoured EB-PVD TBC on a PW4000 second stage blade", *PhD Dissertation Worcester Polytechnic Institute* Worcester, MA Jan 2002

22. Thornton JA. High Rate Thick Film Growth. *Annual Review of Material Science*; 239-260 (1977)

23. "Vapor Phase Intelligent Processing of Thermal Barrier Coatings Agreement No. MDA972-95-3-0039" *IPM-PVD Consortium* May 31, 2000

24. Powell, C.F. "Physical Vapor Deposition" *Vapor Deposition* ed. By Powell, C.F., Oxley, J.H., and Blocher,Jr.,J.M., (1966) p.25-61

25. Movachan, B.A. and Demchishin, A.V. "Study of the Structure and Properties of Thick Vacuum Condensates of Nickel, Titanium, Tungsten, Aluminum Oxide and Zirconium Dioxide *Fiz. Met. Metall*., 28 [4] 83-90 (1969)

26. Schultz, U., Oettel, H. and Bunk, W. "Texture of EB-PVD Thermal Barrier Coatings Under Variable Deposition Conditions" *Zeitschrift fur Metallkunde* 87 488-492 (1996)

27. Sohn, Y.H., Biederman, R.R., and Sisson Jr., R.D. "Microstructural Development in physical vapor- deposited partially stabilized zirconia thermal barrier coatings*" Thin Solid Films* [250] 1-7 (1994)

28. Schultz, U., Schmucker, M. "Microstructure of Zro2 thermal barrier coatings applied by EB-PVD" *Materials Science and Engineering* A276 1-8 (1999)

29. Terry, S.G., Litty, J.R., and Levi, C.G., " Evolution of Porosity and Texture in Thermal Barrier Coatings Grown by EB-PVD," In; *Elevated Temperature Coatings: Science and Technology III_TMS*, Warren ,PA 1999, pp 13-26.

30. Bernier J., Fontecchio M., Maniruzzaman M.d, Sisson Jr. R.D. "Microstructure Evolution of EB-PVD TBCs on Cylindrical Surfaces". *The 26th Annual International Conference on Advanced Ceramics and Composites (Symposium II) Jan 13-18, 2002*, Cocoa Beach, FL. (accepted for publication)

31. Bauer, V.E., "Fiber Texture" *Transaction of 9th National Vacuum Symposium* (1962) p.35-44

32. Van Der Drift, A. "Evolutionary Selection, A Principle Governing Growth Orientation in Vapor-Deposited Layers" *Philips Res. Reports*, vol.22(1967) p.267-288.

33. Bernier, J.S., Weir, W.C.S. , Sisson, Jr R.D., Bose S., "Deposition Rates of EB-PVD TBCs on Cylindrical Surfaces", *The 26th Annual International Conference on Advanced Ceramics and Composites (Symposium II)* Jan 13-18, 2002, Cocoa Beach, FL. (accepted for publication)

Chapter III

Article #1

"DEPOSITION RATES OF EB-PVD TBCS ON CYLINDRICAL SURFACES"

By
J.S.Bernier, W.C.S. Weir, M. Fontecchio, R.D. Sisson, Jr., and S. Bose

Presented at the 26th Annual International Conference on Advanced Ceramics and Composites, Jan. 13-18, 2002 Cocoa Beach, FL accepted for publication in the *Ceramic Engineering and Science Proceedings*.

DEPOSITION RATES OF EB-PVD TBCS ON CYLINDRICAL SURFACES

J.S.Bernier, W.C.S. Weir, M. Fontecchio, R.D. Sisson, Jr.
Materials Science & Engineering Program
Mechanical Engineering Dept
Worcester Polytechnic Institute
Worcester, MA 01609

S.Bose
Materials & Processing Engineering
Pratt & Whitney
East Hartford, CT 06108

ABSTRACT

The coating thickness profiles for EB-PVD TBCs deposited on stationary cylinders have been experimentally measured and theoretically modeled using Knudsen's cosine law of emissions {1}. A comparison of the experimental results with the model reveals that the model needs to be modified to account for the sticking coefficient as well as a ricochet factor. These results are also discussed in terms of the effects of substrate temperature on the sticking coefficient, the ricochet factor, and coating density.

1. INTRODUCTION

It has been shown that increasing the high-pressure turbine inlet temperature in a gas turbine aircraft engine can dramatically improve fuel economy and thrust to weight ratios {2-4}. However, the material properties of the gas turbine blade limit how high the inlet temperature can be raised. In an attempt to raise high-pressure turbine inlet temperatures beyond the melting point of the blade, gas turbine designers have been using ceramic Thermal Barrier Coatings (TBCs) . The TBCs insulate the turbine blades and allow them to run cooler {5}.

A method of applying this coating on a turbine blade is done through Electron Beam Physical Vapor Deposition (EB-PVD). EB-PVD relies on the free diffusion of YPSZ vapor in a vacuum to transport the coating material from the source to the part being coated. During the EB-PVD coating process, the turbine blade is suspended in a vacuum chamber over a YPSZ vapor source or ingot that is melted by an electron beam. As the coating vapors diffuse throughout the vacuum chamber and condense on the part, the YPSZ TBC is formed {6}.

A model has been created that predicts EB-PVD TBC thickness. The model is a modification of Knudsen's cosine law of emissions {6}. To develop the model, several experiments were conducted in the EB-PVD coating chamber. The experiments were conducted by depositing a TBC at varying heights over the ingots onto flat plates, cylindrical surfaces, and turbine blades.

In this study, the model prediction for coating thickness is compared with the experimental data on a cylinder surface, as a function of angular position on the cylinder and position (x,y,z) in the coating chamber. The results are discussed in terms of

substrate temperatures effect on the sticking coefficient, the ricochet factor and coating density.

2. EXPERIMENTAL PRODECURE

A Thermal Barrier Coating (TBC) comprised of Partially Stabilized Zirconia with 7wt% Y_2O_3 (YPSZ) was deposited by EB-PVD onto .3048m long, .0254m diameter stationary cylindrical rods. The cylindrical rods were made of Hastelloy X with a diffusion aluminide bond coat. In each experiment, a cylinder was positioned horizontally in the EB-PVD coater at a specific height above vapor source. The vapor source consisted of two cylindrical ingots. Each ingot was positioned at a specific distance from the cylinder ends as shown in Figure 1. A vacuum was applied to reduce the coating chamber pressure. Table 1 presents the cylinder height data with respect to the ingot's surface for each experiment.

Table 1: Experimental Cylinder Height Data

Experimental #	***Cylinder Height (m)***
90	Baseline + 0.0142
91	Baseline + 0.0397
92	Baseline + 0.0651
93	Baseline + 0.0254
95	Baseline
97	Baseline

When the coating process was complete, the cylinders were cut into twelve .0254m segments as shown in Figure 1. The odd numbered segments were mounted, polished, and marked according to the experiment. The positive and negative numbers below the cylinder represent the side of the cylinder that was polished. The numbers are opposite in sign because the sections should mirror each other according to the geometry of the EB-PVD chamber and fixture.

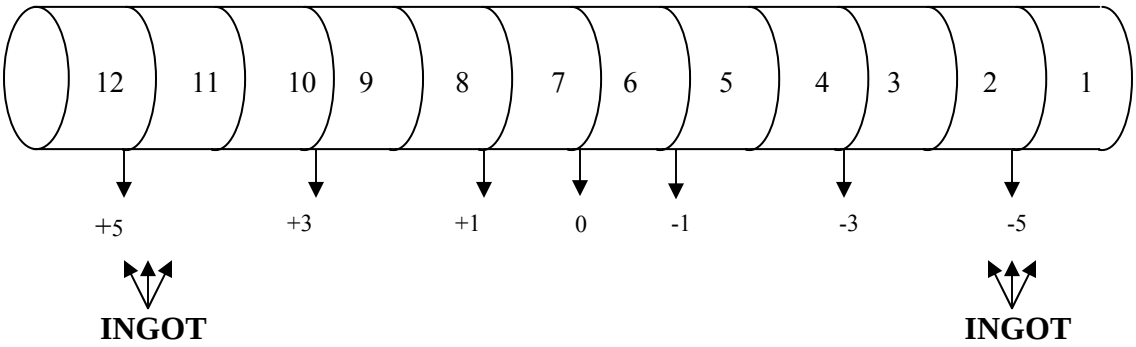

Figure 1: Orientation of Cylinder to the Ingots and Identification of Cylindrical Sections

The TBC thickness was measured at selected angular positions on the cylinder for each mounted section. This was done by placing a .0254m diameter, 360° protractor over the polished cylinder cross-section and placing a mark every 22.5 degrees. Zero degree corresponded to the top of the cylinder, where no TBC had been deposited. The bottom of the cylinder was where the thickest coating deposited, which corresponded to the 180° position. Figure 2 presents a diagram representing a cylinder section with the marked angular positions.

After all the angles were marked, each section was viewed under an optical microscope at 200X magnification. A photomicrograph was taken of each marked angle between 90 and 270 degrees. Coating was observed to be deposited a few degrees above the 90 and 270-degree marks, but with very low density and thickness. The angular marks made on each segment allowed for the angle location to be known when viewing the coating thickness under the microscope. The coating thickness was measured from

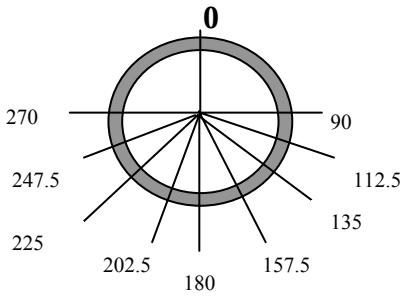

Figure 2: Marked Angular Positions on the Cross Section of the Cylinder

photomicrographs as seen in Figure 3. The measurements were verified with a photomicrograph of a calibrated ruler with 2.54×10^{-5} meter divisions. This thickness was measured using the same a 2.54×10^{-5} -meter ruler. At angles where large TBC thickness variation occurred, an average of 5 points was taken.

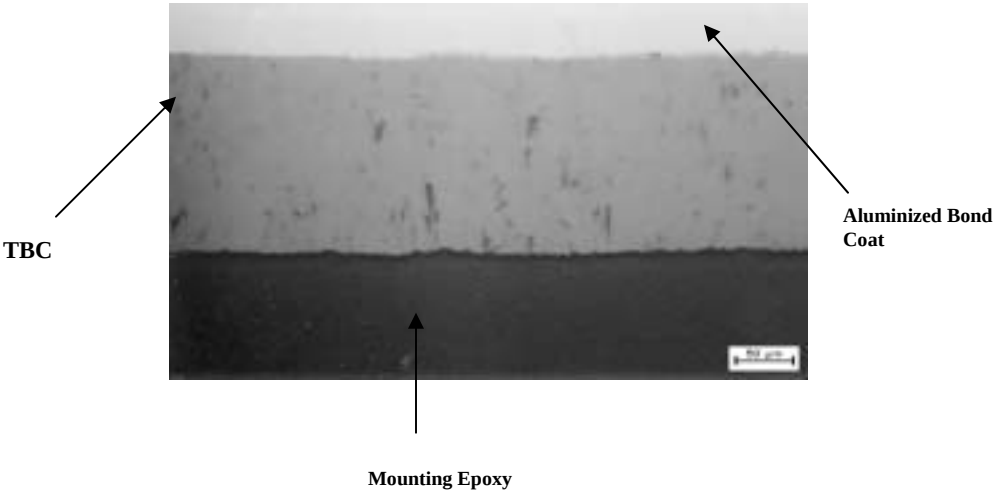

Figure 3: TBC photomicrograph at 180 degrees

The coating thicknesses were measured at the selected angles. These values were compared to the Knudsen model prediction for thickness on a cylinder {1}. The model predicts coating thicknesses at varying distance and angles in a PVD coater as seen in Figure 4.

The TBC thickness predictions were calculated using a Visual Basic program model of Knudsen's cosine law of emissions which states {6}:

$$d = \left[\frac{M_e}{\rho_{coating}} \left(\frac{\cos\theta \cdot \cos\phi}{\pi \cdot r^2} \right) \right]$$

d = Coating Thickness(m)
M_e = Mass of the ingot evaporated (0.35kg)
$\rho_{coating}$ = Density of coating (6050 kg/m^3) (Ref 6&8)
r = Radial distance from emitted to received surfaces(m)
θ = Angle between the radial distance and received surface normal (degrees)
ϕ= Angle between the radial distance and emitted surface normal (degrees)

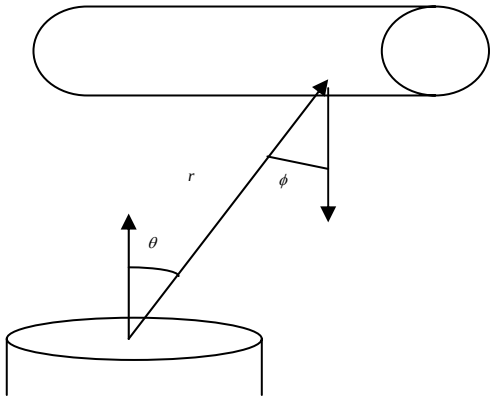

Figure 4: Prediction Model for TBC Deposited on a Cylinder

The Visual Basic program takes into consideration the height on the cylinder above the ingot surface through a radial distance. The angles are taken into consideration through the values of θ and ϕ. Figure 5 shows how the measured coating thickness varies from the predicted thickness as a function of angular position for experiment 90. The thickest coating is deposited at the bottom of the cylinder and decreases as the angular position changes. In all experiments the predicted thickness is greater than the measured thickness at angular positions close to the bottom of the cylinder (i.e. 180 degrees). The greater the angular position from the 180-degree mark, the better the agreement with the model.

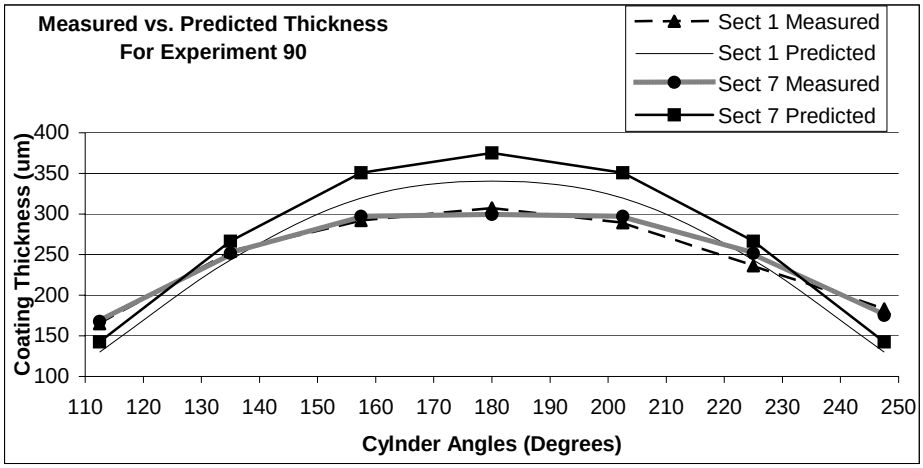

Figure 5: Measured Thickness vs. Predicted Thickness for Exp 90

The area fraction density (AFD) of the TBC was calculated on selected sections and angles using Contexvision image analysis software for experiments 90,91,92,93,and 95.

Determining the sections and angles in each experiment has been previously described. Area fraction density was determined at angles of 112.5, 135, 157.5, 180, 202.5, 225, and 247.5 degrees. At angles where the TBC had fallen off, no density data was recorded for the entire section. Density was not calculated at angles of 90 and 270 because the coating thickness was less than 5 μm and an accurate calculation was not possible. As angular positions move away from the 180-degree mark on the cylinder surface, the coating density decreases {9}. Table 2 shows the sections in each experiment at which the area fraction density was calculated.

Table 2: Sections Which Area Fraction Density Was Calculated

Experimental #	Sections
90	All
91	1,2
92	3,5,7,9,11
93	All
95	All

3. RESULTS AND DISCUSSION

The coating thickness of each marked section was measured at the selected angles and compared to the cylinder model based on Knudsen's law of emissions at the same angles. The measured vs. predicted thickness data of each section was compiled and plotted for each experiment. An example is shown in Figure 6 for measured thickness vs. model thickness for experiment 90. As seen in Figure 6 the experimental thickness is approximately 0.91 times the model thickness. This coefficient is in agreement with previous work done on flat plates {7}. Table 3 shows how the R^2 and the slope(m) in y=mx, varied at different cylinder heights.

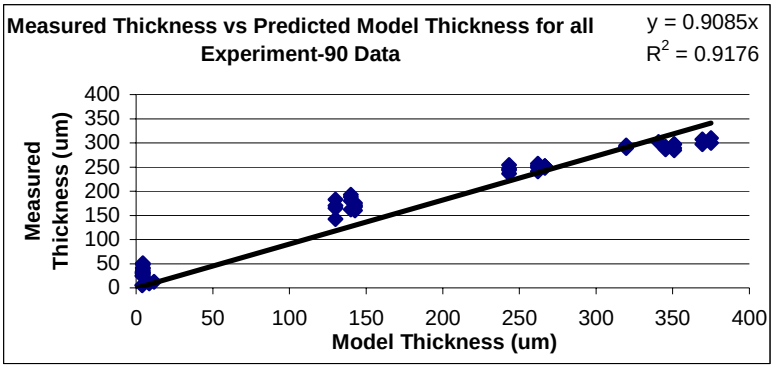

Figure 6: Measured vs. Model Thickness for Experiment 90

Figure 7 presents a compilation of all cylinder data plotted. The plot shows there is a good correlation between the model and the measured data. However, there are a few factors that are not considered in the model in order to get a y vs. x correlation. In Figure 7, the slope of the line is less than 1, indicating there are some additional factors not accounted for in the model prediction. These factors are believed to be the sticking coefficient/probability and a factor involving the ricochet effect {10}. These factors, along with many others, could account for the model and the measured thickness discrepancies.

Table 3: R^2 and Y Variation for Experiments with Respect to Height

Experiment	R^2	*Slope (y=)*	Height (m)
90	0.918	0.909x	Baseline + 0.0142
91	0.878	0.897x	Baseline + 0.0397
92	0.819	0.863x	Baseline + 0.0651
93	0.851	0.726x	Baseline + 0.0254
95	0.924	0.802x	Baseline
97	0.913	0.818x	Baseline

In EB-PVD deposition, not all the ZrO_2 and ZrO molecules that strike the surface will stick. However, some molecules may strike the chamber walls and ricochet, striking the substrate and finally stick. Some of the molecules that do stick to the substrate surface may sublime due to high substrate temperatures.

The substrate temperature influences the surface energy of the sticking molecules. The temperature of the substrate is not well controlled in these experiments and is difficult to monitor. The chamber temperature may be known, but does not reflect the temperature of the substrate surface where the coating is being deposited. However, for several experiments where the cylinder height was low, the Hastelloy metal exhibited incipient melting (Exp 95 and 97). The temperature, therefore, was above the melting temperature of the Hastelloy X.

A possible cause for substrate temperature differences is radiation-heating coming from the EB-PVD coater walls or the fixture above the cylinder. As the EB-PVD process continues, coatings on the walls build up causing a higher temperature within the vacuum chamber and thus a higher substrate temperature. The closer the fixture is to the cylinder, the higher the substrate temperature.

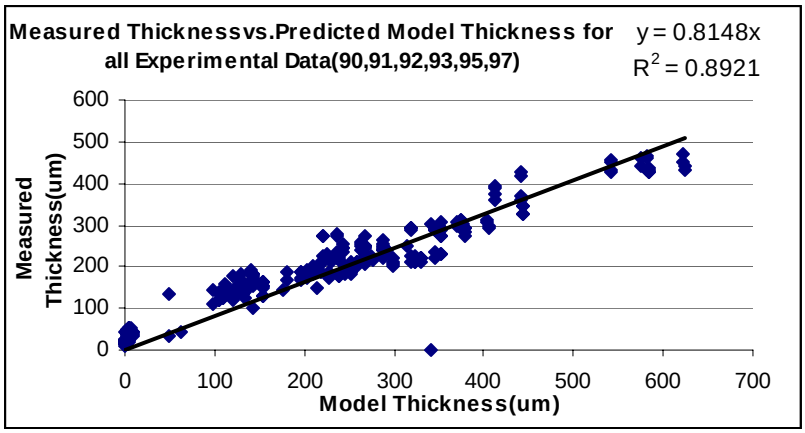

Figure 7: Measured vs. Model Thickness for all Experimental Data

Another reason the substrate temperature may vary is due to condensation energy. At high deposition rates, the condensation energy can produce appreciable substrate heating. When a thermally vaporized atom condenses on a surface, it releases energy causing sublimation {10}. If variations in the substrate temperature between experiments and/or each experiment exist, these variations may explain why the measured and predicted coating thicknesses do not agree. Substrate temperature is a factor associated with surface energy, which relates to the sticking coefficient and film growth characteristics. The high substrate temperature, where incipient melting of the Hastelloy occurred, may also have caused sublimation of some deposited vapor flux molecules changing the coating thickness.

Another variable the model must take into consideration is the ricochet factor. In EB-PVD, a high vacuum is applied (0.00133Pa) so the vaporizing material travels in a straight line between the vaporizing source and the substrate (i.e., line-of-sight deposition). The outer most point on the ingot has a "line-of-sight " deposition point somewhere on the cylinder above the 90-degree mark. That point is the last possible place coating could be deposited on the cylinder. If coating is found above the

cylindrical tangent points ricochet has taken place. Figure 8 depicts how the ricochet effect may have taken place in the previous experiments.

Density of the coating deposited was also measured at selected angler positions and compared to the theoretical density (6050kg/m^3) {6 & 8}. Figure 9 shows how coating density varies with cylinder height and angle positions. The figure on the left presents experiment 95(baseline height) while the figure on the right presents experiment 92 (baseline + 0.0651m). The lower the cylinder height and the less change in angular position from the bottom of the cylinder, the greater the coating density. This is may be true because a higher substrate temperature is found closer to the ingot vapor source promoting a greater surface energy {11}. Also angular position changes from the bottom of the cylinder promote a greater degree of self-shadowing based on the vapor incidence angle {9}. The microstructure associated with the TBC density on cylindrical surfaces is presented in a comparison paper {9}.

It is combination of the sticking coefficient and the ricochet effect that causes the experimental thickness to be between 73 and 91 percent of the model prediction. The Knudsen's model assumes that every molecule that strikes the substrate surface will stick.

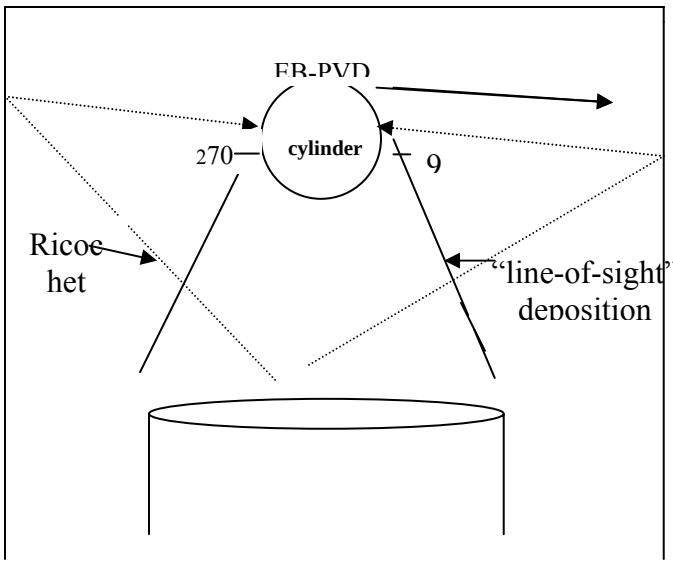

Figure 8: Ricochet Effect Diagram

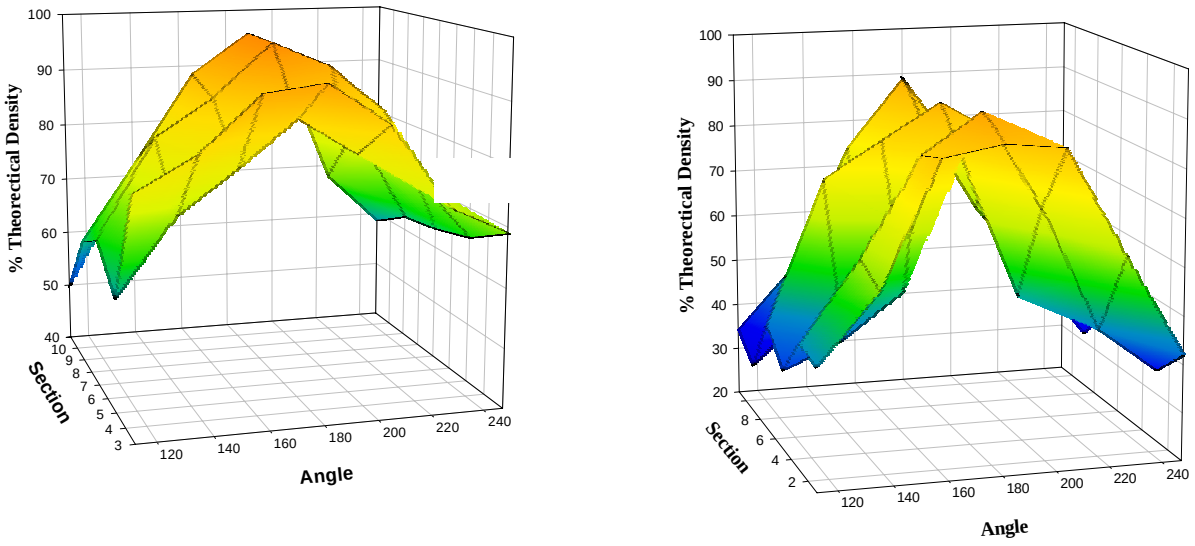

Figure 9: Density Variations According to Height and Angular Position Exp 95 (left) and Exp 92 (right)

4. CONCLUSION

1. The model for predicting coating thickness on cylinders must to be modified to take into consideration substrate temperature (sticking coefficient) and the ricochet effect. The new prediction model is:

$$d = 0.81\left[\frac{M_e}{\rho_{coating}}\left(\frac{\cos\theta\cdot\cos\phi}{\pi\cdot r^2}\right)\right]$$

2. Coating thickness and density decrease as the angular position changes from the bottom of the cylinder.

REFERENCES

1. Glang R. Vacuum Evaporation. In: Maissel LI, Glang R, editors. *Handbook of Thin Film Technology*. New York: McGraw-Hill; 1970. p 1-3 to 1-123.
2. Wortman DJ, Duderstadt EC, Nelson WA. "Bond Coat Development for Thermal Barrier Coatings," *Journal of Engineering for Gas Turbines and Power* 1990;112:527-30.
3. Johnson CA, Rud JA, Bruce R, Wortman D. "Relationships between residual stress, microstructure and mechanical properties of electron-beam physical vapor deposition thermal barrier coatings," *Surface and Coating Technology* 1998;108-9:80-85.
4. Demeray RE, Fairbanks JW, Boone DH. "Physical Vapor Deposition of Ceramic Coatings for Gas Turbine Engine Components," *Journal of Engineering for Power 1982*.
5. Sheffler KD, Gupta DK. "Current Status and Future Trends in Turbine Application of Thermal Barrier Coatings," *Journal of Engineering for Gas Turbines and Power* 1988;110:605-9.
6. Weir, W.C.S., " Development of a rule based software system for the fabrication of a contoured EB-PVD TBC on a PW4000 second stage blade", *PhD Dissertation Worcester Polytechnic Institute* Worcester, MA Jan 2002
7. Weir, W.C.S., Sisson R.D. Jr, Bose, S., "Rule-Based software tool to specify the manufacturing process parameters for a contoured EB-PVD coating," *Intelligent Systems in Design and Manufacturing III, Bhaskaran Gopalakrishnan, Angappa Gunasekaren, Editors, Proceedings of SPIE* Vol 4192 (2000)©@ 2000 SPIE 0277-786X/00/$1500, p 330-337.
8. Scardi Paolo ,Leoni, Matteo." Microstructure and Heat Transfer Phenomena in Ceramic Thermal Barrier Coatings" *Journal of American Ceramic Society* 84 [4] 827-835 (2001)

9. Bernier J., Fontecchio M., Maniruzzaman M.d, Sisson Jr. R.D. "Microstructure Evolution of EB-PVD TBCs on Cylindrical Surfaces". *The 26th Annual International Conference on Advanced Ceramics and Composites (Symposium II) Jan 13-18, 2002*, Cocoa Beach, FL. (accepted for publication)

10. Mattox, Donald M. "Atomistic Film Growth and Some Growth Related Film Properties*," Handbook of PVD Processing* Westwood, N.J.: Noyes Publications; 1998. pp. 444-489.

11. Thornton JA. "High Rate Thick Film Growth". *Annual Review of Material Science* 1977 p.239-260.

Article #2

"MICROSTRUCTURAL EVOLUTION OF EB-PVD TBCS ON CYLINDRICAL SURFACES"

By

J.S.Bernier, Md. Maniruzzaman, M. Fontecchio, R.D. Sisson, Jr., and S. Bose

Presented at the 26th Annual International Conference on Advanced Ceramics and Composites, Jan. 13-18, 2002 Cocoa Beach, FL accepted for publication in the *Ceramic Engineering and Science Proceedings.*

MICROSTRUCTURAL EVOLUTION OF EB-PVD TBCS ON CYLINDERICAL SURFACES

J. Bernier, Md. Maniruzzaman, M. Fontecchio, R.D. Sisson Jr.,
Materials Science & Engineering Program
Mechanical Engineering Dept
Worcester Polytechnic Institute
Worcester, MA 01609

S.Bose
Materials & Processing Engineering
Pratt & Whitney
East Hartford, CT 06108

ABSTRACT

The microstructures of EB-PVD TBCs have been characterized as a function of angular position and cylinder height on stationary cylindrical surfaces in the coating chamber. The microstructures were evaluated using x-ray diffraction for qualitative crystallographic texture as well as by optical microscopy and scanning electron microscopy for crystal column growth morphology. The results revealed several very strong crystallographic textures as well as a variety of crystal growth morphology.

1. INTRODUCTION

Thermal barrier coatings (TBC) are applied to components used in high temperature, high-pressure environments. TBC systems consisting of Yttria partially stabilized ZrO_2 (YPSZ) on an aluminum containing metallic bond coat, are found on hot components of various heat engines such as turbine blades. The TBCs help increase in performance, durability, and efficiency by allowing for a higher combustion temperature, lower metal surface temperature, and reduced cooling airflow {1}. Thermal barrier coatings are applied to turbine blades by a process known as electron beam physical vaporization (EB-PVD). This process produces a columnar crystal microstructure with varying column diameters {2}.

PVD structure maps have been developed to relate coating microstructure to homologous temperature (T/Tm), where T is the substrate temperature and Tm is the melting point of the TBC in degrees Kelvin. A simple structure map developed by Movchan and Demchishin is shown in Figure 1. The microstructure of EB-PVD coatings is influenced by many parameters including, shadowing, surface and volume diffusion, vapor incidence angle, and desorption {3}. These parameters are related to the substrate temperature, gas pressure, and the degree of ionization in the vapor phase {4}. The microstructure of the TBCs is roughly predicted by either the Thornton {4} structure diagram or the Movchan and Demchishin diagram {5}. Surface curvature, roughness, and substrate movements may emphasize the shadowing effects and initiate subsequent deviations from the predictions of these diagrams {6}. The shape, which a crystal acquires by any growth process, depends on the nucleation conditions and the availability and the surface diffusion of atomic species on crystallographic planes. There is a general

consensus that the columns of growth are monocrystalline, where a single phase is involved, with crystallographic texture controlled by the process parameters. It has also been reported that vapor deposition results in the preferential growth of coatings {7}. The resulting crystallographic texture has been explained by "evolutionary selection" {6, 7} which states that the crystal with the fastest growing direction orients itself towards the vapor source {7}. The "evolutionary selection" depends on the processing parameters of the deposition rate.

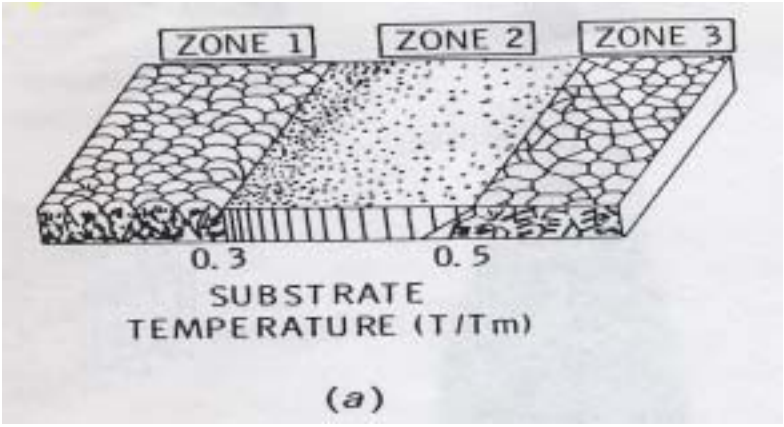

Figure 1: Structure map for deposited TBC film structure vs. homologous temperature. Ref{ 5}

This study focuses on the microstructure of YPSZ TBC deposited by the EB-PVD onto a stationary cylinder. The results are explained through analysis of optical and scanning electron microscopy. Crystallographic texture results are given by comparing the powder x-ray diffraction pattern to the x-ray diffraction pattern of the deposited TBC, at the given angular positions on the cylinder.

2. EXPERIMENT PROCEDURE

Thermal Barrier Coating (Partially Stabilized Zirconia 7wt% Y_2O_3) was deposited by EB-PVD onto 0.3048m long, 0.0254m diameter stationary cylindrical rod. The rod was made of Hastelloy X with a diffusion aluminide bond coat. The cylinder was positioned

horizontally in the EB-PVD coater at a specific height above the ingots. The coating is deposited under a high vacuum (References 8 provides more information on the EB-PVD coater and process).

When the coating process was complete, the cylinder was cut into twelve 0.0254m segments, of which every odd numbered segment was metallurgically mounted, polished, and marked according to the experiment. Figure 2 shows a diagram of how a cylinder was cut and labeled. The positive and negative numbers below the cylinder represent the side of the cylinder that was polished. The numbers are opposite in sign because the sections mirror each other by the geometry of the EB-PVD chamber and fixture {9

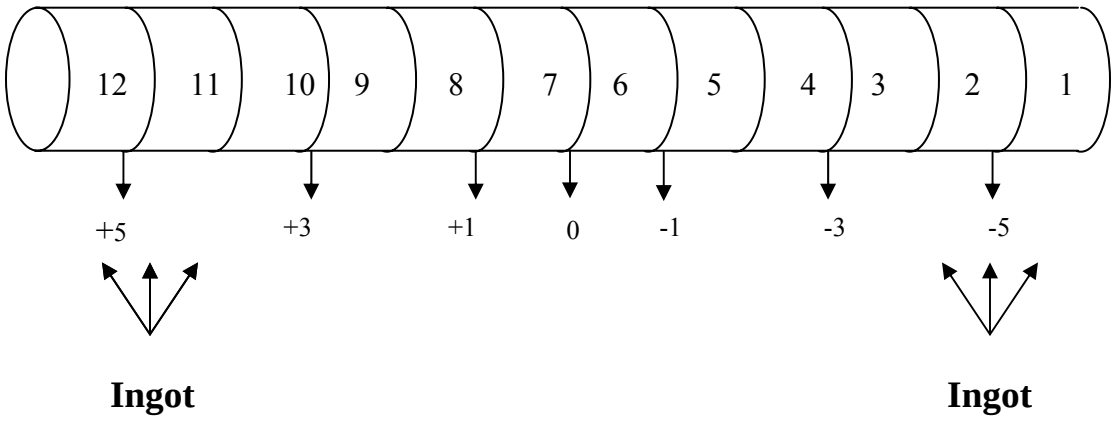

Figure 2: Orientation of Cylinder to the Ingots and Identification of Cylindrical Sections

Once the cylinder sections were cut and labeled, the even sections had their angular positions marked. This was done by placing a 0.0254 diameter, 360° protractor over the end of cylinder cross-section and placing a mark every 30 degrees. Zero degrees corresponded to the top of the cylinder, which no TBC had been deposited. The bottom of the cylinder was where the thickest coating was deposited, which corresponded to the 180° position. Figure 3 presents a diagram representing the marked angular positions

on a cylinder cross-section looking through a top view. Positions 270 thru 90 degrees were not labeled because they were not analyzed for this paper.

The coated sections were investigated by scanning electron microscopy (SEM) and optical microscopy for each angular position. X-ray diffraction (XRD) phase analysis was performed for each angle. The patterns were then compared with that of the starting YPSZ powder in order to determine crystallographic texture. When recording the x-ray patterns, Cu K α radiation was used at a rate of 2 degrees per minute. The angular range in which the patterns were taken was from a two-theta value of 20 to 160 degrees.

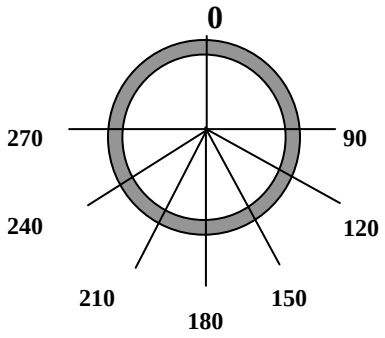

Figure 3: Marked Angular Positions on the Cross Section of the Cylinder

3. RESULTS & DISCUSSION

3.1. X-Ray

X-ray patterns were taken on the previously specified angles and sections. The results were compared with the powder pattern of YPSZ in order to determine if crystallographic texture existed. Figure 3 presents an example of an as deposited TBC x-ray diffraction pattern from section 4 at angular position of 180 degrees. The reason for the low intensity readings is that the line up slit was used for taking patterns on the curved surface. Figure

4 presents an x-ray diffraction pattern of the YPSZ ingot powder, used as evaporation source. The same line up slit was used to take the powder diffraction pattern but the powder was of fine randomly oriented particles.

From figures 4 and 5 is evident that crystallographic texture exists in the EB-PVD coatings. Table 1 shows the planes of greatest normalized intensity for each section at the specified angles. The table also shows the planes of greatest normalized intensity for the YPSZ powder. Planes with a normalized intensity less than 30% were not indexed.

As shown in Table 1 a variety of crystallographic textures were observed for different sections and angular positions. The textures observed at 180 degrees (i.e. when the coating is growing normal to the cylinder surface) are of the (220), (420), (531), and (311) types. This data is in general agreement with previous work {1}. At angles where the coating is not growing perpendicular to the cylinder surface normal (150,120 degrees ect), several other textures were observed including the (620), (200), and (111) type. However, as the x-ray diffraction patterns were taken normal to the cylinder surfaces, (i.e. not normal to the columnar growth direction), no conclusions can be made at this time with regard to growth direction of the crystals {1}.

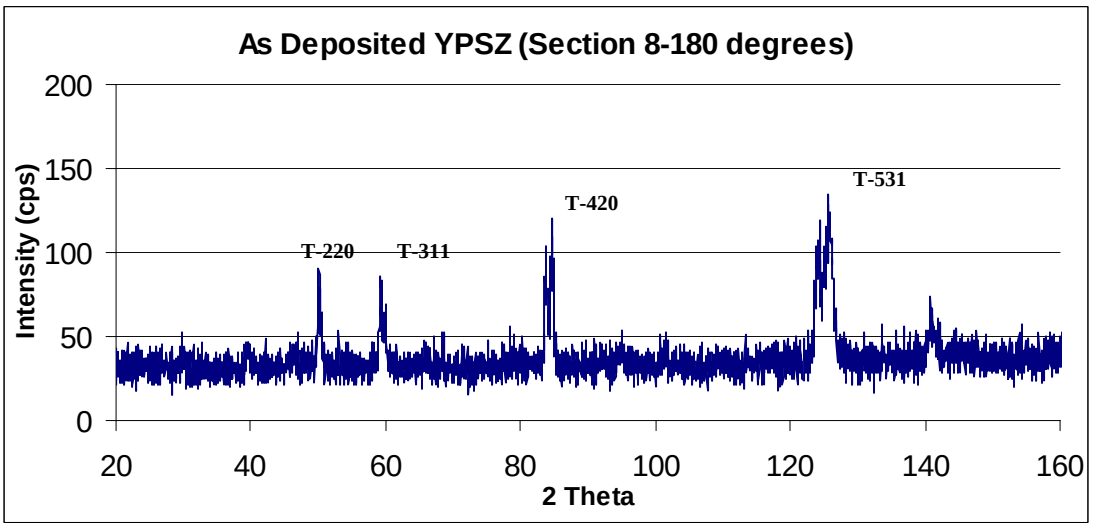

Figure 4: Example of as deposited X-ray pattern for YPSZ

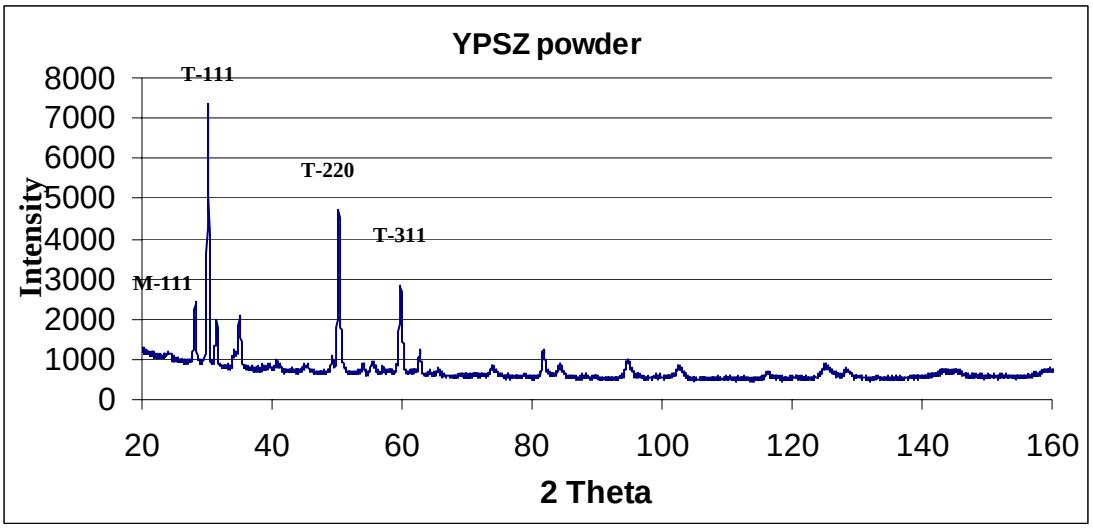

Figure 5: XRD pattern for powder YPSZ

A tetragonal system was identified on the deposited YPSZ. This was based on a comparison between the x-ray diffraction pattern and JCPDS card number 17-0923. The YPSZ powder x-ray diffraction pattern revealed the powder ingot material to be monoclinic.

Table 1: Planes of greatest normalized intensity from XRD Patterns

Angle	90	120	150	180	210	240	270	Powder
Sect	plane-I/Io	plane-I/Io	plane-I/Io	plane-I/Io	plane-I/Io	plane-I/Io	plane-I/Io	plane-I/Io
2	311-100% 200-47% 511-35%	511-100%	620 -100% 420-50%	220-100%	620-100% 420-60%	200-100% 400-43%	311-100% 620-45% 200-40% 220-35%	111-100% 220 -59% 311-30%
4	200-100% 511-98% 400-52% 311-40% 220-40%	200-100%	620-100% 420-56%	220-100%	620-100%	200-100% 400-47%	311-100%	111-100% 220 -59% 311-30%
6	311-100% 200-78% 220-68%	200-100%	620-100%	420-100% 531-52%	620-100%	200-100% 400-41%	511-100% 311-43% 220-35%	111-100% 220 -59% 311-30%
8	311-100%	511-100%	620-100%	531-100% 420-86% 200-57% 311-53%	511-100% 311-65% 620-46%	200-100% 400-38%	311-100%	111-100% 220 -59% 311-30%
10	511-100% 200-49% 311-47% 220-37%	200-100%	620-100% 311-59%	311-100% 531-86% 420-65%	620 -100% 311-73% 511-65%	200-100% 400-40%	311-100%	111-100% 220 -59% 311-30%
12	311-100% 220-54% 200-37% 111-37%	511-100% 620-35%	511-100%	420-100%	420-100% 620-39%	511-100% 311-44%	111-100% 311-63%	111-100% 220 -59% 311-30%

3.2 Microscopy

Optical photomicrographs were taken of sections seven and eleven. The photomicrographs were adjacent to sections six and twelve, respectively, and were taken at the same angular positions as were used for the x-ray patterns. Figure 5a thru 5f show how section location and angular position influence columnar growth and density. Angular position has a large effect on the coating density. The further away from the 180-degree mark on the cylinders the more porous the deposited coating becomes. It can also be noted that section location may also have an effect on the coating density. From the photomicrographs, section 7-180 appears to be more porous than section 11-180.

SEM photomicrographs were taken of sections 4, 6, and 12 at the same angular positions as were used for the x-ray diffraction patterns and adjacent to the optical photomicrographs. The surface features of the EB-PVD coatings as a function of angular position and location on the cylinder are presented in figure 6. As shown in figures 6b, 6e, and 6h, the bottom of the cylinder (i.e.180 degrees) displays a dense, faceted morphology while the sides of the cylinder exhibit a less dense and "tube like" columnar structure with inter-columnar gaps. The inter-columnar gaps are due to self-shadowing associated with the high vapor incidence angle with respect to the normal.

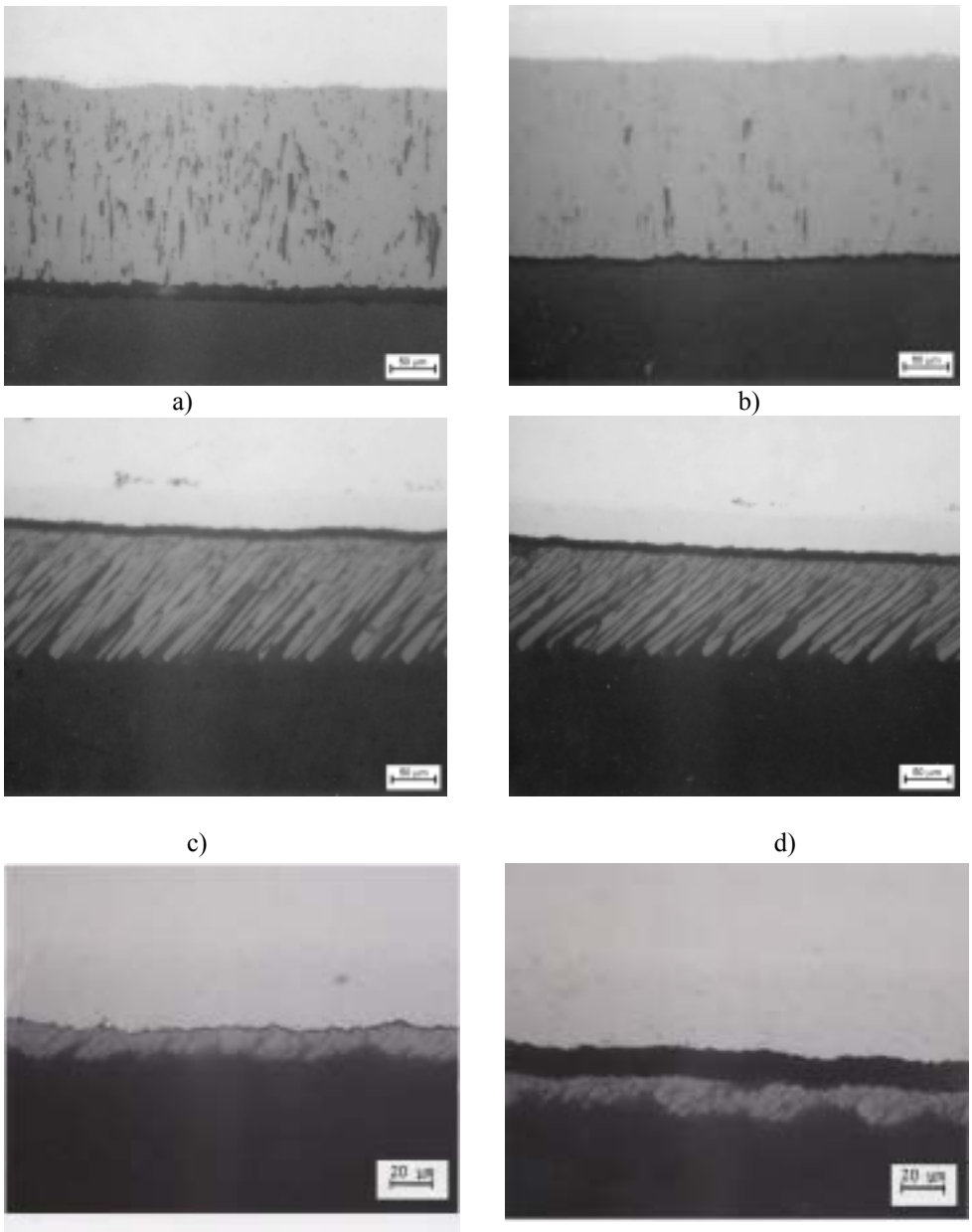

Figure 5: Optical photomicrographs showing column orietation a) sect 7 @180degrees b) sect 11 @ 180degrees c) sect7 @ 120 degrees d) sect 11 @ 120 degrees e) sect 7 @90 degrees f) sect 11 @ 90 degrees

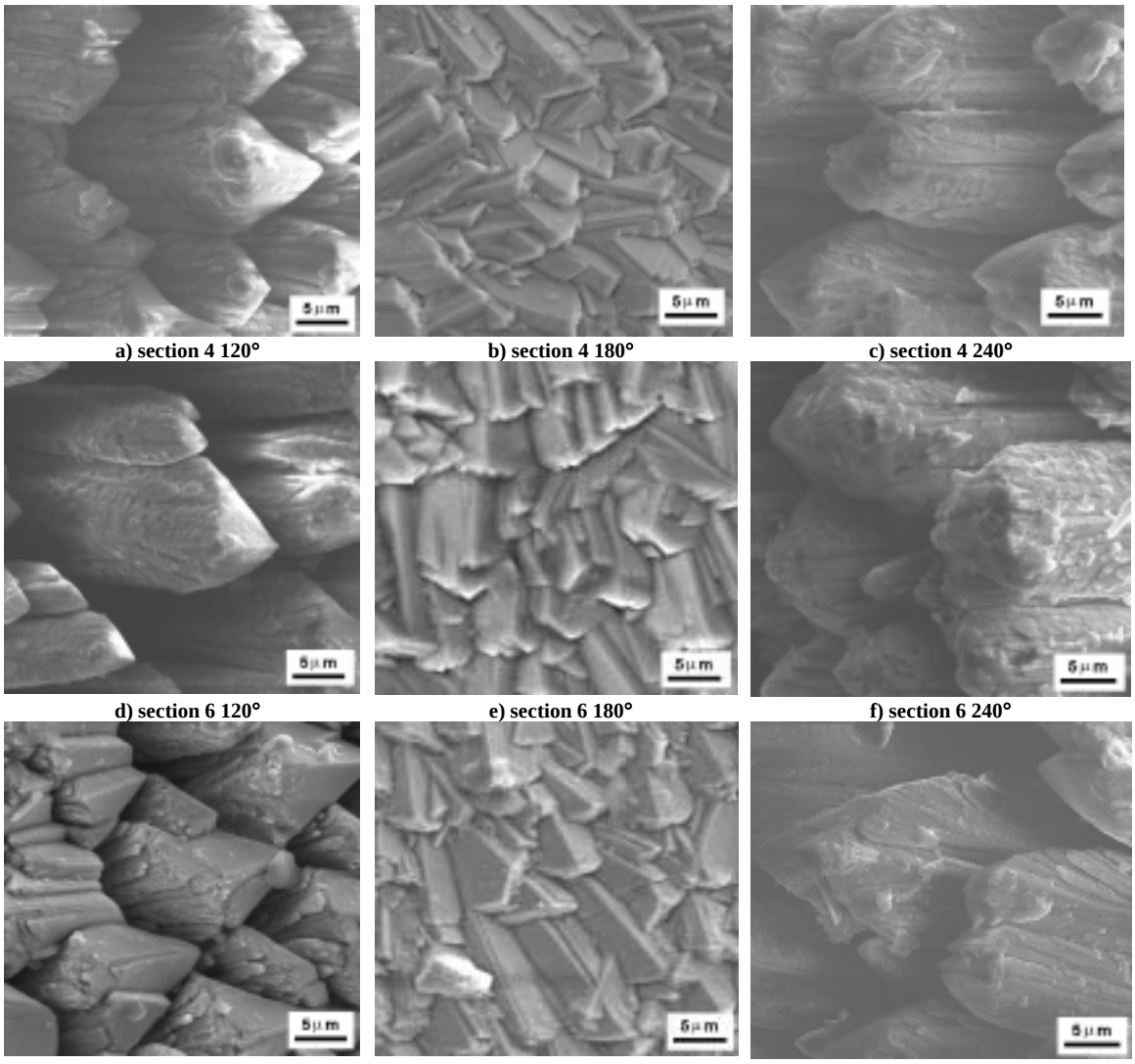

a) section 4 120° b) section 4 180° c) section 4 240°

d) section 6 120° e) section 6 180° f) section 6 240°

g) section 12 120° h) section 12 180° i) section 12 240°

Figure 6: Microstructures of the deposited TBC at different cylinder sections and angles

In general the microstructure of the cross sections that are symmetrical to each other with respect to the midpoint of the cylinder, (i.e. +/- 1, +/- 3, +/- 5) as seen in Figure 1 are very similar. That is the microstructure of sections 12 and 1 or 10 and 3 are nearly identical to each other. However, microstructure variations are seen between sections where coating was deposited directly above the ingots (i.e. sections 12 and 1) and sections where coating was deposited between the ingots (i.e. sections 8,4,6).

Microstructure variation also occurs between non-symmetrical sections (i.e. sections 12 and 6) as seen in Figure 6.

REFERENCES

1. Sohn, Y.H., "Thermal Barrier Coatings," *Characterization and Life Prediction of Vapor Deposited Partially Stabilized Zirconia Thermal Barrier Coatings*, Worcester Polytechnic Institute Worcester, MA (1993) p4

2. Schultz U., Fritscher K., Ratzer-Scheibe H-J. , Kaysser W.A. and Peters M. *Thermocyclic Behavior of Microstructurally Modified EB-PVD Thermal Barrier Coatings*, Materials Science Forum 957-964 (1997)

3. Schultz U., Fritscher K., Peters M. "EB-PVD Y203-and CeO2/Y2O3-stabilized zirconia thermal barrier coating s-crystal habit and phase composition" *Surface and Coatings Technology* [82] 259-269 (1996)

4. Thornton JA. High Rate Thick Film Growth. *Annual Review of Material Science*; [7] 239-260 (1977)

5. Movachan B.A. and Demchishin A.V., "Study of the Structure and Properties of Thick Vacuum Condensates of Nickel, Titanium, Tungsten, Aluminum Oxide and Zirconium Dioxide *Fiz. Met. Metall*., 28 [4] 83-90 (1969)

6. Terry, Scott G. , Litty, Jennifer R., and Levi, Carlos G. " Evolution of Porosity and Texture in Thermal Barrier Coatings Grown by EB-PVD," In; *Elevated Temperature Coatings: Science and Technology III TMS*, Warren ,PA 1999, pp 13-26.

7. Sohn Y.H,. Biederman R.R and Sisson Jr, R.D. "Microstructural Development in physical vapor- deposited partially stabilized zirconia thermal barrier coatings" *Thin Solid Films* [250] 1-7 (1994)

8. Weir, W.C.S., " Development of a rule based software system for the fabrication of a contoured EB-PVD TBC on a PW4000 second stage blade", Ph D Dissertation Worcester Polytechnic Institute Worcester, MA Jan 2002

9. Bernier, J.S., Weir, W.C.S. , Sisson, Jr R.D., Bose S., Deposition Rates of EB-PVD TBCs on Cylindrical Surfaces, *The 26th Annual International Conference on Advanced Ceramics and Composites (Symposium II)* Jan 13-18, 2002, Cocoa Beach, FL. (accepted for publication)

Article # 3

"***CRYSTALLOGRAPHIC TEXTURE AND COLUMN GROWTH DIRECTION OF EB-PVD TBCs DEPOSITED ON FLAT SURFACES IN A MULTIPLE INGOT COATING CHAMBER ***"

By

J.S.Bernier, G. Levan , S. Bose, Md. Maniruzzaman, and R.D. Sisson, Jr.,

Submitted to Acta Materialia on May 18, 2002

Crystallographic Texture and Column Growth Direction of EB-PVD TBCs Deposited on Stationary Flat Surfaces in a Multiple Ingot Coating Chamber

J.S.Bernier[1], G. Levan[2], S. Bose[2] , Md. Maniruzzaman[1], and R.D. Sisson, Jr[1].

[1]Materials Science & Engineering Dept
Worcester Polytechnic Institute
Worcester, MA 01609

[2]Materials & Process Engineering
Pratt & Whitney
East Hartford, CT 06108

ABSTRACT:

The crystallographic texture (i.e. preferred orientation) of EB-PVD TBCs has been experimentally determined by comparing pole figure data with measured column growth angles. The column growth angle is defined as the angle at which the TBC column grows with respect to the surface substrate. It was found that TBC coating deposited on a flat surface directly above an ingot exhibited <220> single crystal type crystallographic texture. While coatings deposited between the two ingots and off the centerline exhibited a <311>-type single crystal texture. Coatings deposited at the far corners of the coating chamber revealed either a <111>-fiber texture or <311> single crystal type texture. The microstructures of the specimen cross-sections reveal that the column growth angle and vapor incidence angle are in reasonable agreement and that columns grow towards the closest vapor source. However, for flat surfaces located between the ingots and off center of the line, the dual ingots supplied two nearly equal vapor incidence angles that caused a complex and confused column growth direction. Position changes in the coating chamber cause substrate temperature, column growth angle and vapor incidence angle changes, all of which have been found to influence crystallographic texture in TBC coatings. The Bragg-Brentano x-ray diffraction analysis revealed a variety of textures (i.e. crystallographic planes that are parallel to the substrate surface) with the most predominant planes being the (220), (311), (420), and (620). Comparison of XRD data and pole figure analysis revealed that for cases where

the crystal growth is not normal to the substrate, the most intense diffraction plane from the x-ray diffraction pattern is the plane parallel to the surface and not the preferred growth direction.

KEYWORDS: Crystallographic Texture, Microstructure, Growth Direction, Vapor Incidence Angle, EB-PVD, Thermal Barrier Coatings, Zirconia, and PSZ

1. INTRODUCTION

Zirconia partially stabilized with 7% Yttria (YPSZ) is the current state-of-the-art material for thermal barrier coatings (TBCs) used in high- pressure high-temperature turbine environments [1]. TBCs are usually comprised of an insulating ceramic top coating, which reduces metal temperature, and a bond coat, which provides oxidation and corrosion protection. The bond coat also allows for better adhesion of the TBC to the superalloy substrate [2].

Currently, the YPSZ TBCs are applied to turbine blades and vanes by two methods, Electron Beam Physical Vapor Deposition (EB-PVD) and Plasma Spraying (PS) [3]. EB-PVD processed TBCs offer significant benefits over PS TBCs because of their unique columnar microstructure [3]. The columnar microstructure provides outstanding resistance against thermal shock and tolerance to mechanical strains, which are associated with high temperature, high-pressure turbine blades. PS coatings exhibit a laminar structure that consists of splats with cracks parallel to the surface structure, which affects cyclic life of the TBC [4].

During the EB-PVD coating process, there are several process parameters that have an effect on the coating thickness, density, crystallographic orientation, and microstructure [5]. These process parameters are the chamber pressure, part position in the chamber, substrate temperature, electron beam current, and deposition rate, which are controlled by the melt pool temperature, substrate rotation, and substrate height [6].

The microstructure of EB-PVD coatings is influenced by surface and volume diffusion, desorption, and shadowing [7,8] which are related to substrate temperature, chamber pressure, and gas phase ionization [3,7,8]. The microstructure of TBCs is roughly predicted by either the Thornton structure diagram [8] or the Movchan and Demchishin diagram [9]. At elevated temperatures surface diffusion of vapor molecules deposited on the substrate surface is accelerated causing a larger column diameter and a more regular microstructure [3]. It has also

been found in literature [10] that as temperature increase the morphology of YPSZ changes from "flat pyramidal" surfaces to "rooftop" surfaces indicated by minimizing surface energy.

Surface curvature, roughness, and rotation cause self-shadowing effects and cause deviations in morphology from the predictions of these diagrams [11]. Self-shadowing refers to the simple geometric interaction between irregular growing surface and the angular directions of the arriving molecules [8]. Rotational speed has also been found to affect the microstructure by changes in column diameter, coating thickness, and porosity [3,12]. It has been reported [3] that at low substrate temperatures and low rotational speeds columns exhibit a small diameter that are arranged more irregular causing a higher degree of porosity. At high substrate temperatures and rotational speeds columns are larger are more regular and parallel over their length with a decrease in porosity.

It has also been reported that vapor deposition results in the preferential growth of coatings [13]. This preferential growth causes crystallographic texture, which has been explained by "evolutionary selection" [13]. The "evolutionary selection" states that in the absence of re-evaporation from the growing surface, the column growth direction is dictated by the direction of the incoming vapor flux and competition occurs between crystals growing at different rates. The crystal with the fastest growing orientation takes over and dominates the crystallographic texture [10]. The direction of the incoming vapor flux is related to the vapor incidence angle of the growing crystallites and therefore has an affect on the crystallographic texture of PSZ coatings [13,14,15]. It has been found in literature [13,14,15] that changes in vapor incidence angle (VIA) or substrate temperature have an effect on the type of crystallographic texture and the orientation of that texture. Clarke [10] found that as substrate temperature is increased texture changed from predominately a <111> fiber texture to either a <200> fiber texture or a <111>, <200> single crystal texture. Schultz [15] found that <113> fiber texture existed for coatings deposited directly above an ingot, but as the VIA changed either a <111> or <110> fiber texture was found. He also

observed that the loss of fiber texture was observed for high VIA and high deposition rates. Substrate temperature is also found to influences a crystallites growth rate which, influences texture. Growth rate of crystallites is influenced by parameters such as surface energy, surface and volume diffusion, and grain boundary mobility all of which are related to substrate temperature [15]. At elevated substrate temperatures, there is greater mobility of the condensing coating molecules. This causes the molecules to move into a more stable or lowest energy configurations that result in a higher degree of ordering in the lattice causing crystallographic orientation [11,15].

The present study focuses on the microstructure and crystallographic texture of YPSZ TBC deposited by the EB-PVD onto stationary flat surfaces from two ingots containing the same YPSZ composition. The results are presented in terms of scanning electron microscopy of the coated surfaces and cross-sections, pole figures, and x-ray diffraction.

2. EXPERIMENTAL PRODECURE

A YPSZ (7wt% Y_2O_3) Thermal Barrier Coating was deposited onto stationary flat tabs from two ingots by EB-PVD process. The flat tabs were 2.54 cm by 2.54 cm and made of Hastelloy X with a diffusion aluminide type bond coat. Prior to coating, the tabs were placed in a flat plate fixture (Figure 1) [16], which could hold a total of 210 tabs. However, for the present experiments, fifty tabs were set in the coating fixture at random locations and placed in the coating chamber at a nominal height above the two ingot vapor source. The flat plate fixture was centered between the 2 ingots in the coating chamber and an identification number was stamped on the backside upper left hand corner of each tab. This allowed for tab orientation to be known when placed in the fixture. When the tab was placed in the fixture, the stamped number was oriented towards the A1 position. Five additional experiments were also conducted with the same process parameters and tab locations, making a total of six experiments for a reproducibility study.

When the coating process was complete, six tabs were selected from the reproducibility study experiments. The tabs were from positions F6,E7, I12, B11, H2, and C19. Figure 2 represents the selected tabs location in the fixture with respect to ingot locations. The tabs had x-ray diffraction and pole figure analysis performed to determine crystallographic orientation. X-ray diffraction was conducted using Cu Kα radiation, at a rotation rate of two thetadegrees per minute with a two-theta range of 20 to 160 degrees. The crystallographic plane parallel to the substrate surface for the YPSZ coating was determined for each tab from the XRD pattern.

Pole figures were obtained using a Philips ATC-3 texture cradle using Cu radiation with a nickel filter in the diffracted beam. The texture data were collected out to a psi angle of 70° and corrected for contributions from background and defocusing. The data were then analyzed using Philips X'Pert texture software in order to produce complete pole figures for crystallographic orientation type.

The surface morphology of the YPSZ tabs was characterized by using scanning electron microscopy (SEM). Finally, each selected tab was cut twice, 90 degrees apart and mounted in Buehler Epo Thin Low Viscosity Epoxy as shown in Figure 3. The mounted samples were polished for SEM cross-section microscopy to determine the column growth angle and the rotation of that angle from the x-axis (Figure 3) with respect to the closest vapor source.

The column growth angle was determined by measuring the angle of growth on surfaces A and B in Figure 3 from the SEM photomicrographs. The angles from the A and B surfaces were then used to compute an overall growth angle. The vapor incidence angle (VIA) and rotation of that angle from sample to sample were also determined for each tab based on geometric principles of the coating fixture and tab location within the coating chamber. These data were then compared to each other and then to the pole figure analysis data to determine the primary growth planes.

3. RESULTS

3.1 Scanning Electron Microscopy of the Top Surfaces of the TBC Coating

Scanning Electron Microscopy was performed on each tab to characterize the surface morphologies. From the surface morphology (Figures 4 and 5) it appears that the closer the vapor source is to the location of the tab, the larger the scale of the morphological features. The larger size features may be associated with the thicker coating that is deposited directly above or between the vapor source [17]. Tab F6 (Figure 4a&b) located directly above an ingot appears to have "rooftop" type morphology with the random arrangement of the individual surface grains with respect to the growth direction. Tab E7 (Figure 4c&d) presents the same type morphology as tab F6, but the arrangement of the individual surface grains with respect to the growth direction appears to be oriented in a certain direction. Tabs I12 (Figure 4e&f) and B11 (Figure 5a&b), both located further away from the vapor source, generally show faceted or "rooftop" morphology in which the "rooftops' are smaller than tabs F6 or E7. However, tab I12 appears to have a certain orientation of the individual surface grains while B11 exhibits random arrangement of the surface grains. The two tabs, H2 (Figure 5c&d) and C19 (Figure 5e&f), located outside the central coating zone exhibit smaller "rooftop" pyramid structures located between larger "rooftop" structures. They also appear to have an orientation of the individual surface grains with respect to the incoming vapor direction. Individual surface grains that are oriented in a certain direction can be associated with tabs receiving coating primarily from the closest vapor source. However, tabs I12 and B11, in general, receive coating from both ingots. Tab B11's random morphology may be attributed to being equidistant from both vapor sources while tab I12 is located closer to one vapor source causing the individual surface grains to be oriented toward that ingot. The morphology present from the samples, has also been observed by U. Shultz [14,15], Sohn [13,14], Levi [11], and Bernier [18]. The differences among the tab morphologies can easily be seen to be a function of position in the coating chamber.

3.2 Scanning Electron Microscopy of the Coating Cross Sections

SEM photomicrographs were taken on the A and B surfaces (Figure 3) of the selected tabs cross-sections and are presented in Figures 6-8. A protractor was used to measure the angle between the substrate surface and the general column growth direction on both surfaces. The column growth angle (CGA) was determined using the measured angle information and is defined as the angle at which the TBC column grows towards the closest ingot with respect to the surface substrate (θ_1 in Figure 9). Table 2 presents the CGA data and the calculated vapor incident angle (VIA) data for each tab with respect to the closest ingot. The VIA is defined as the angle between the surface substrate and the direction of the vapor beam from the center of the closest ingot. The VIA and GCA should be the similar since the columns grow in general at the angle which the vapor hits the substrate surface. The angle of rotation was also determined for both the VIA and the CGA. The angle of rotation is defined as the number of degrees the VIA or CGA is rotated from the tab's x-axis (Figure 3) in order to point towards the closest vapor source. Depending on tab location, the x-axis was considered from the top or bottom of the tab. For example the rotation angle for tab H2 was calculated from the tabs bottom x-axis while for tab C19 the rotation angle was calculated from the top x-axis. The VIA and its rotation angle are calculated from the coating fixture geometry with respect to the tabs location and height from the center of the closest ingot. The angle of rotation for the CGA is determined from the SEM cross-sections of the tabs A & B surfaces. Table 1 gives definitions of all the angles and their rotations mentioned in this paper and how they were determined. In Table 2, a reasonable agreement between the VIA, CGA, and their rotation angles is seen. Overall the crystal growth appeared to be in the general direction of the closest ingot based upon the SEM cross section photomicrographs of each tab and knowing its orientation in the coating fixture. However, tabs B11 and I12 are nearly equidistant from the two vapor sources and therefore no clear VIA could be determined that would be in reasonable agreement with the CGA. Both tabs receive coating

from both ingots making the VIA and the column growth direction a combination of vapor from both ingots. The crystal growth direction of Tab I12 was found to grow in the general direction of ingot 2 (Figure 2) as expected. No clear growth direction or column growth angle could be determined for tab B11 based upon the uncertainty of surface A's cross section photomicrograph. Tabs above an ingot (F6, E7) or in the corners of the coating chamber (C19, H2) receive coating predominately from the closest ingot. This allows the columns to grow in the general direction of the closest ingot at a certain angle. The coating received from the non-predominant ingot may have an effect on the CGA and CGA's rotation angle not correlating exactly with the VIA and VIA's rotation angle.

3.3 Pole Figures

Many authors have revealed a number of different texture types relating to TBCs deposited on rotated and stationary substrates [12,15] through pole figure analysis. Such textures include the <001>, <011>, <113>, and <111> type. Factors such as vapor incidence angle (VIA), substrate temperature, coating thickness, and substrate rotation all have influence the texture of EB-PVD coatings, although no clear relationship has been established [3,11,12,13,14].

Pole figures were determined for 6 stationary tabs from the selected locations in an EB-PVD multi ingot coater. All pole figures were taken on the top layer of the coated surface of the specimens and no texture vs. depth information was obtained in this study. Pole figure data (Figures 10-15) show single crystal type texture and fiber type texture. Single crystal texture happens when all the crystal grains have approximately the same crystallographic orientation (F6,E7, I12,B11, and C19). Fiber texture happens when all the grains are oriented along a growth direction with no preferred orientation in the growth plane- (H2). For tab C19, (Figure 15) a single crystal fiber texture existed although in a previous experiment a <111>-fiber texture was found under the same process conditions. The literature shows that fiber textures are formed at low substrate temperatures [10] and also depend on the VIA [15]. Schulz [15] et al

found that for VIAs greater than 0°, <111> or <110> fiber textures existed with the fiber axis shifted off from the center of the pole figure [15]. However, for specimens coated directly above the vapor source, Shultz [15] found a <113> fiber texture. In this work no fiber textures were found for tabs coated directly above a vapor source (F6,E7) which may be due to a high substrate temperature. Specimens H2 and C19 have a coating geometry that is similar to the stationary coating case because they see one primary vapor flux from the closest ingot. H2 (Figure 14) shows a <111>-fiber texture with the fiber axis ~30° off the center of the pole figure while C19 exhibits single crystal type texture. The specimens are from opposite sides of the coater, and local conditions such as vapor flux/vacuum system interactions and substrate temperature may be playing a role in the different texture types.

Pole figure data were gathered from each tab, for the {111}, {220}, {311}, and {420} type planes. For each plane considered on a tab, the inclination angle from the tab surface ($90-\theta_2$ from Figure 9) and the rotation of that angle towards the closest x-axis was obtained. θ_2 is defined as the number of degrees the specified {hkl} plane is shifted from the center of the pole figure. Pole figure angle information is presented in Table 3. Only the most intense (hkl) plane for a given {hkl} set is indicted in Table 3. For example, the F6 tab has two <420> locations in the pole figure with one being more intense than the other. The most intense (420) plane was selected to appear in the table and is denoted with an "*" in Figures 10-15. In Table 3, the highlighted data represents pole figure angle and rotation data of a particular growth plane that matches fairly well with the CGA and VIA data. The pole figure data also reveals what general direction the columnar growth points (either towards or away from a vapor source).

A comparison of the VIA, CGA, and the highlighted pole figure analysis data is presented in Table 4. Primary growth planes were identifying by comparing the highlighted pole figure data in Table 3 with the VIA and CGA data of Table 2. For a tab where two rows were highlighted,

only one primary growth plane was chosen based on the crystal growth direction. For example, for tab C19 two (hkl) planes match the CGA data fairly well. The (311) plane was chosen because growth plane points back at the primary vapor source matching the CGA data while the (220) plane points away from both vapor sources. For tab F6, the columnar growth is normal to the substrate being located directly above a vapor source. The (220) plane was chosen as the primary growth plane because the (220) plane was the most intense according to the XRD data and match the CGA data. XRD data is taken normal to the substrate surface and matches the pole figure data fairly well. A primary growth plane could not be determined for tab B11 because CGA data information could not be obtained. Overall, there appears to be reasonable agreement between the VIA, CGA, and highlighted pole figure analysis data in order to determine a primary growth plane for different locations within the coating chamber.

Crystallographic texture was also found to vary with coating thickness. Tabs located directly above the vapor source where the thickest coating was received have different type crystallographic texture than tabs that received less coating (C19, H2).

3.4 X Ray Diffraction (XRD)

A method for characterizing texture in EB-PVD coatings is to acquire x-ray diffraction profiles, and then calculating the ratio of the peak heights to determine if a particular set of planes is predominantly parallel to the substrate surface. Figure 16 presents an as deposited YPSZ x-ray diffraction pattern for tab C19. As illustrated in the Figure, the (420) is the strongest peak indicating that the (420) plane is parallel to the substrate surface.

Table 5 shows the planes of greatest normalized intensity for each tab. Planes with a normalized intensity less than 35% are not presented. The texture observed for tab F6 (i.e. when the coating is growing normal to the surface, directly above the ingot) are of the (220) type, is in general agreement with previous work [14, 18]. At tab locations where the coating is not growing parallel to the surface normal (E7, I12, B11, H2 and C19), several other textures were

observed including the (220), (620) and (420) type. However, as the x-ray diffraction patterns were taken normal to the substrate surfaces, (i.e. not normal to the columnar growth direction), no conclusions could be made with regard to growth direction of the crystals based on XRD data alone [15]. X-ray diffraction patterns provide basic texture information, but do not completely describe the exact state of grain orientation in the coating. The pole figure of tab C19 (Figure 14) shows the {420} planes parallel to the surface substrate just as the XRD pattern predicted (Figure16). However, based on the pole figure analysis data and correlating that data with the column growth angle (CGA) and vapor incidence angle (VIA) data, the planes growing parallel to the columnar growth are of (311) type. Therefore, the coating really has <311> type texture not <420>-type texture as predicted by the XRD pattern. Based on the XRD data and the JCPDS card data indicated in Table 4, it is apparent that different type texture exists throughout the coating chamber.

4.0 DISCUSSION

It has been found that the coating morphology, microstructure, and crystallographic texture are a function of position in the two ingot-coating chamber. These variations are due to the effects of vapor incidence angle (VIA) and substrate temperature. Surfaces directly above an ingot (Tabs F6 & E7) experience a perpendicular VIA as well as the highest temperature in the coating chamber due to direct radiation for the ingot. These coatings exhibit a normal column growth angle and a <220>-column growth direction with single crystal texture. Surfaces away from both ingots, in the corners of the coating chamber (Tabs H2 and C19) experienced a lower VIA and substrate temperature. These coatings revealed either <311> or <111> column growth directions with fiber or single crystal texture. The coating surface between the ingots and off the centerline (Tab I12) experienced an intermediate substrate temperature and two distinct VIAs. The coating revealed a <311>-growth direction with single crystal texture and a "confused" microstructure.

The experimental results may be applied to the coating textures, morphologies and microstructures of turbine blades and vanes that are rotated during the coating process in a multiple ingot coater. During rotation each surface will experience all VIAs as well as variation in substrate temperature. These variations in VIA and temperature will cause the coating to tend to exhibit a variety of crystallographic textures and microstructures, including density variations, that have been present in this paper.

The well known "layered' [15] microstructure of commercial EB-PVD TBCs depends on the rotational velocity and process parameters, which influence the thickness of the deposited coating. The variation in temperature and VIA due to rotational velocity may cause differences in the crystallographic texture and microstructure within each layer. These variations in crystallographic texture and microstructure may have a significant effect on the mechanical and thermal properties of these coatings.

5.0 SUMMARY:

1. Overall surface morphology and crystallographic texture are influenced by tab location within a multi ingot coating chamber. The crystallographic texture differences are due to temperature changes and VIA changes within the coating chamber.

2. For non-rotated tabs located directly above a vapor source (F6,E7), <220>-type texture exist. This is in agreement with XRD data because XRD data is taken normal to the substrate and the columnar growth is normal to the substrate when deposited directly above a vapor source.

3. For non-rotated tabs located between and off center of two vapor sources a <311>-type texture was found based on the columnar growth data and pole figure analysis data. However, variation between the vapor incidence angle(VIA) data and columnar growth data existed due to the fact that VIA data only takes into consideration coating being received from one ingot not two.

4. For non-rotated tabs located outside the central coating zone either single crystal or fiber crystallographic texture existed. Texture type is caused by substrate temperature and VIA changes throughout the coating chamber.

5. Based on pole figure analysis and columnar growth data, the primary growth plane grows towards the nearest vapor source in a multi ingot coater. The growth direction controlled by which vapor flux hits the coating surface first, causing self shadowing of the second vapor source. Growth direction may point to the primary vapor source because more vapor is deposited from the primary vapor flux than the secondary

ACKNOWLEDGEMENT

The authors are grateful to Mr. Steven M. Burns and Tyrus Royal of Pratt & Whitney for assistance in EB-PVD coating experiments and to Mark F. Zelesky for his encouragement. The Pratt&Whitney/WPI Learning Factory supported this project.

References

1. Schultz,U., "Phase Transformation in EB-PVD Yttria Partially Stabilized Zirconia Thermal Barrier Coatings during Annealing" *J.American Ceramic Society* 83[4] 2000, p.904-910.

2. Schultz, U., Fritscher, K., Leyens, C. "Two-Source Jumping Beam Evaporation for Advanced EB-PVD TBC Systems" *Surface and Coatings Technology* 133-134 (2000) p.40-48.

3. Schultz,U., Fritscher, K., Ratzer-Scheibe, H.J., Kaysser, W.A. and Peters, M. "Thermocyclic Behavior Of Microstructurally Modified EB-PVD Thermal Barrier Coatings" *Materials Science Forum* vols. 251-254 (1997) P.957-964.

4. Beele, W., Marijnissen, A. and Van Lieshout, A. " The Evolution of Thermal Barrier Coatings -status and upcoming solutions for todays key issues" *Surface and Coatings Technology* 120-121 (1999) p.61-67.

5. Weir, W.C.S., Sisson R.D. Jr, Bose, S., "Rule-Based software tool to specify the manufacturing process parameters for a contoured EB-PVD coating*," Intelligent Systems in Design and Manufacturing III, Bhaskaran Gopalakrishnan, Angappa Gunasekaren, Editors, Proceedings of SPIE* Vol 4192 (2000)©@ 2000 SPIE 0277-786X/00/$1500, p 330-337.

6. "Vapor Phase Intelligent Processing of Thermal Barrier Coatings" *IPM-PVD DARPA* May 31, 2000

7. Schultz U., Fritscher K., Peters M. "EB-PVD Y_20_3-and CeO_2/Y_2O_3-stabilized zirconia thermal barrier coating s-crystal habit and phase composition*" Surface and Coatings Technology* [82] 259-269 (1996)

8. Thornton J.A. "High Rate Thick Film Growth". *Annual Review of Material Science*; [7] 239-260 (1977)

9. Movachan B.A. and Demchishin A.V., "Study of the Structure and Properties of Thick Vacuum Condensates of Nickel, Titanium, Tungsten, Aluminum Oxide and Zirconium Dioxide *Fiz. Met. Metall*., 28 [4] 83-90 (1969)

10. Heydt P., Luo C., and Clarke D. "Crystallographic Texture and Thermal Conductivity of Zirconia Thermal Barrier Coatings Deposited on Different Substrates

11. Terry, Scott G. , Litty, Jennifer R., and Levi, Carlos G. " Evolution of Porosity and Texture in Thermal Barrier Coatings Grown by EB-PVD," In; *Elevated Temperature Coatings: Science and Technology III TMS*, Warren ,PA 1999, pp 13-26.

12. Sohn Y.H,. Biederman R.R and Sisson Jr, R.D. "Microstructural Development in Physical Vapor- Deposited Partially Stabilized Zirconia Thermal Barrier Coatings*" Thin Solid Films* [250] 1-7 (1994)

13. Sohn,Y.H. "Characterization and Life Prediction of Physical Vapor Deposited Partially Stabilized Zirconia Thermal Barrier Coatings" M.S. Thesis Worcester Polytechnic Institute, Worcester, MA 1993

14. Schultz, U., Oettel, H. and Bunk, W. "Texture of EB-PVD Thermal Barrier Coatings Under Variable Deposition Conditions" *Zeitschrift fur Metallkunde* 87 488-492 (1996)

15. Schultz, U., Schmucker, M. "Microstructure of Zro2 thermal barrier coatings applied by EB-PVD" *Materials Science and Engineering* A276 1-8 (1999)

16. Weir, W.C.S., " Development of a Rule Based Software System for the Fabrication of a Contoured EB-PVD TBC on a PW4000 Second Stage Blade", Ph D Dissertation Worcester Polytechnic Institute Worcester, MA Jan 2002 SYH thesis

17. Bernier, J.S., Weir, W.C.S. , Sisson, Jr R.D., Bose S., "Deposition Rates of EB-PVD TBCs on Cylindrical Surfaces", *The 26th Annual International Conference on Advanced Ceramics and Composites (Symposium II)* Jan 13-18, 2002, Cocoa Beach, FL. (in the press)

18. Bernier J., Fontecchio M., Maniruzzaman M.d, Sisson Jr. R.D Bose.S. "Microstructure Evolution of EB-PVD TBCs on Cylindrical Surfaces". *The 26th Annual International Conference on Advanced Ceramics and Composites (Symposium II) Jan 13-18, 2002*, Cocoa Beach, FL. (in the press)

List of Figures

List of Tables

Figure 1: Flat Plate Fixture

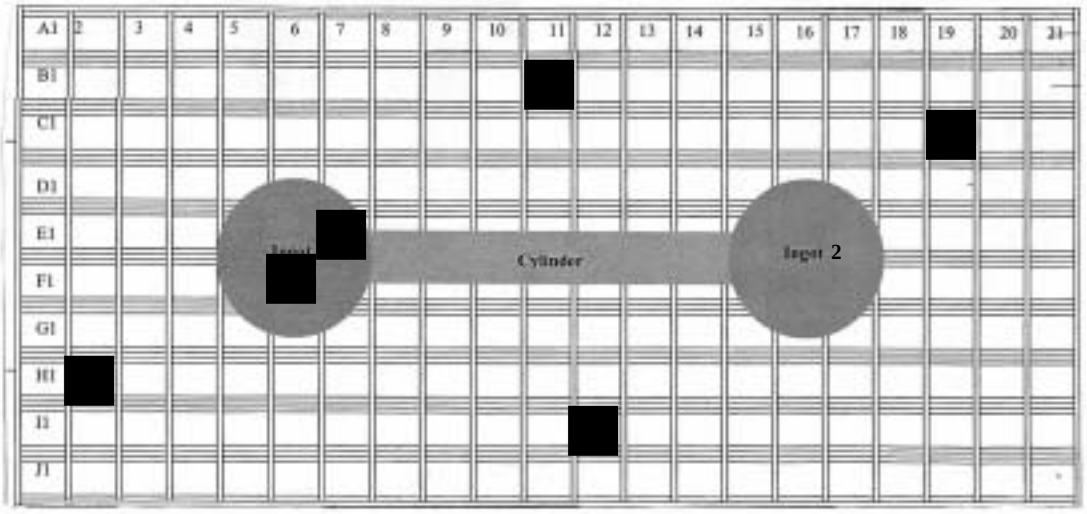

Figure 2: Tab Location in the Flat Plate Fixture

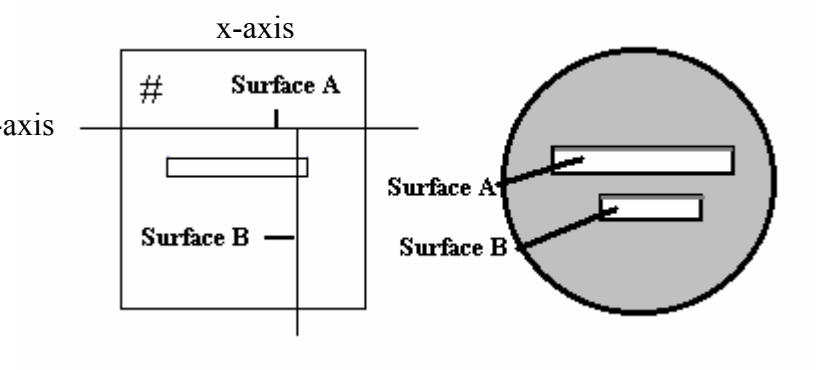

Figure 3: Tab Orientation for Columnar Growth in the Metallographic Section

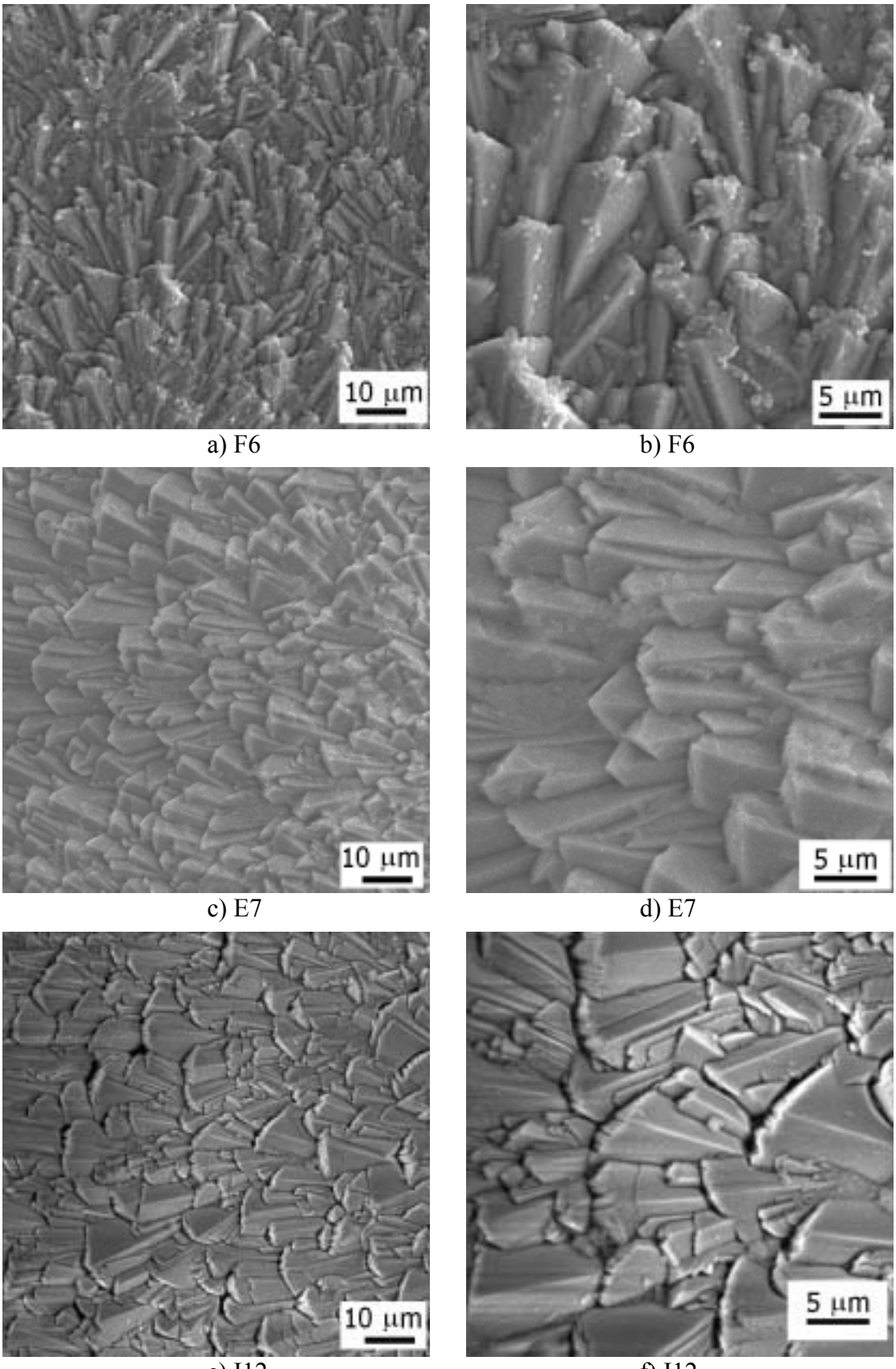

a) F6 b) F6

c) E7 d) E7

e) I12 f) I12

Figure 4: SEM Surface Morphologies (Tabs F6, E7, I12)

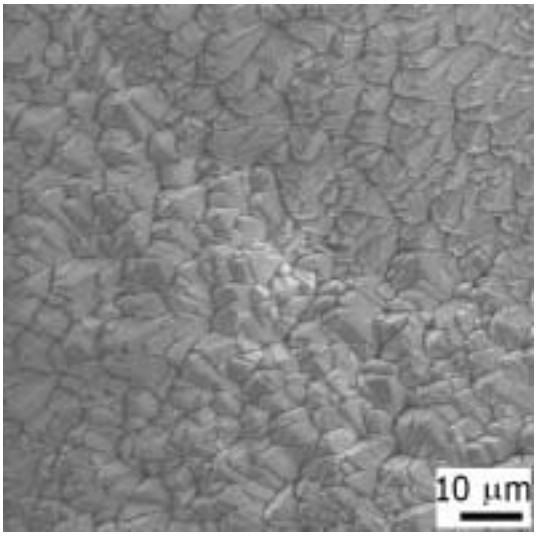

a) B11

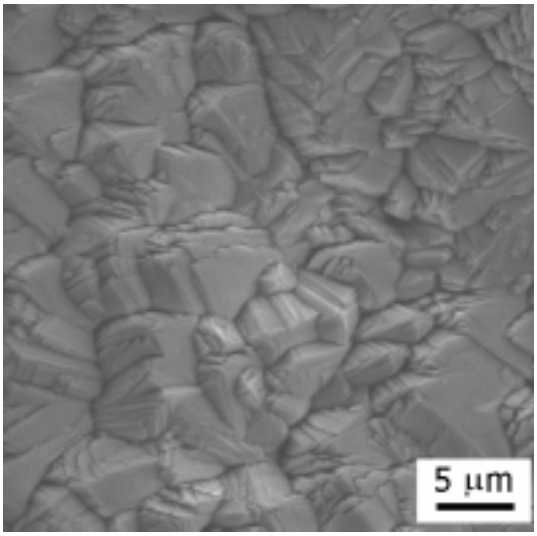

b) B11

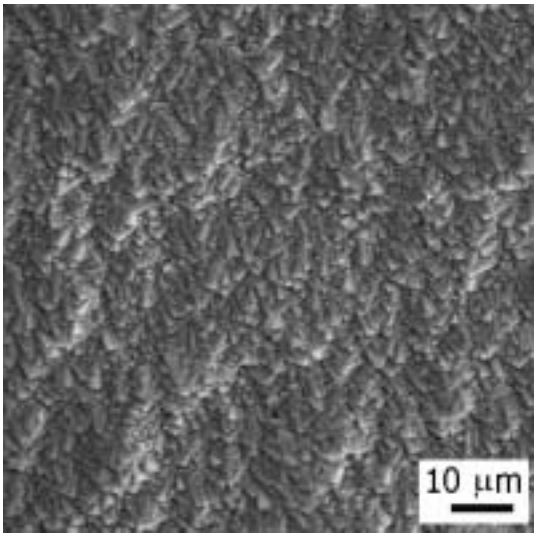

c) H2

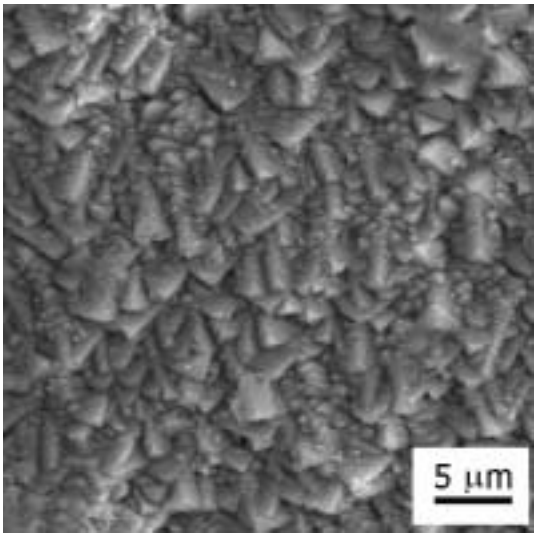

d) H2

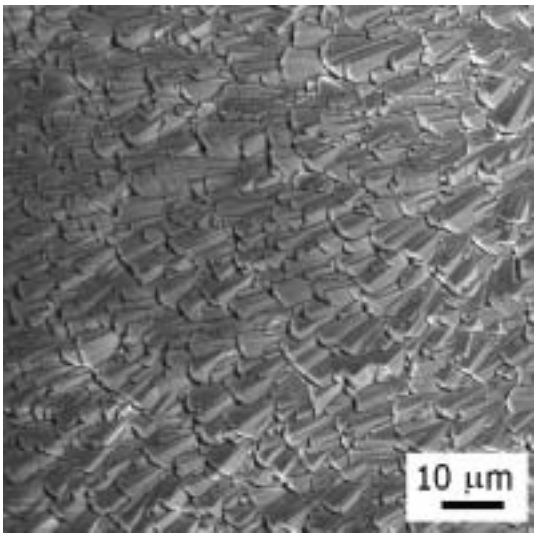

e) C19

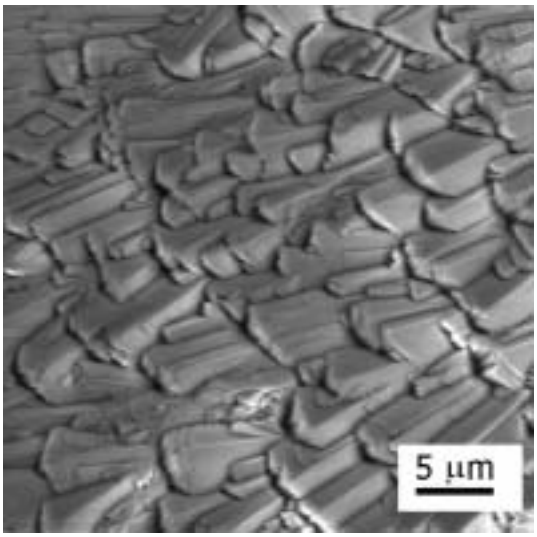

f) C19

Figure 5: SEM Surface Morphologies (Tabs B11, H2, and C19)

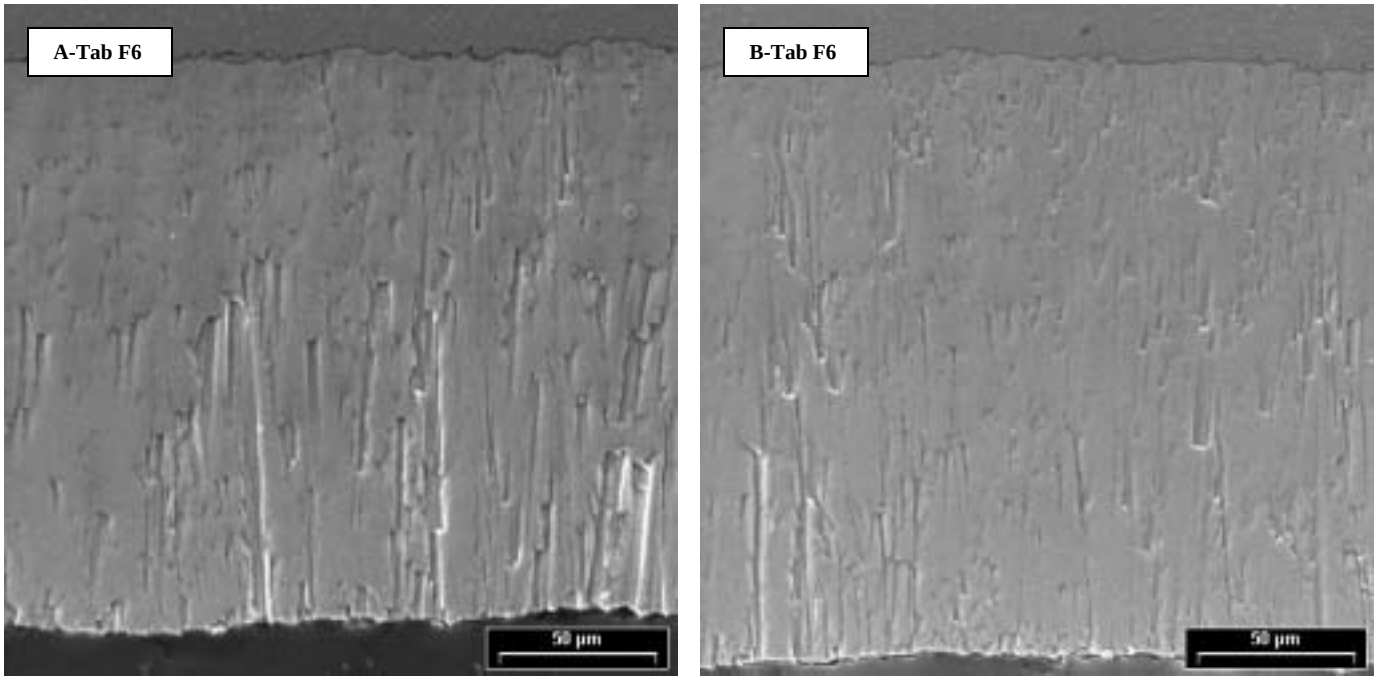

a)

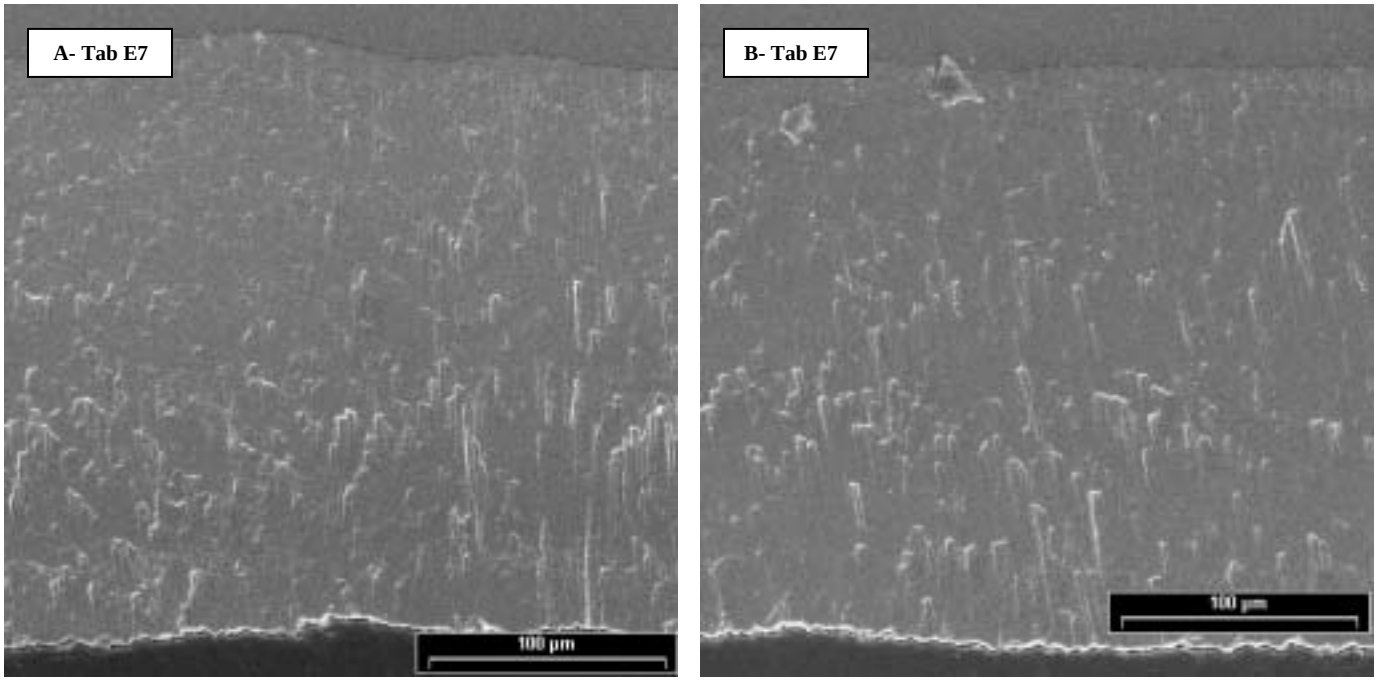

b)

Figure 6: SEM Tab Cross Sections of Surfaces A and B for Tabs F6 and E7

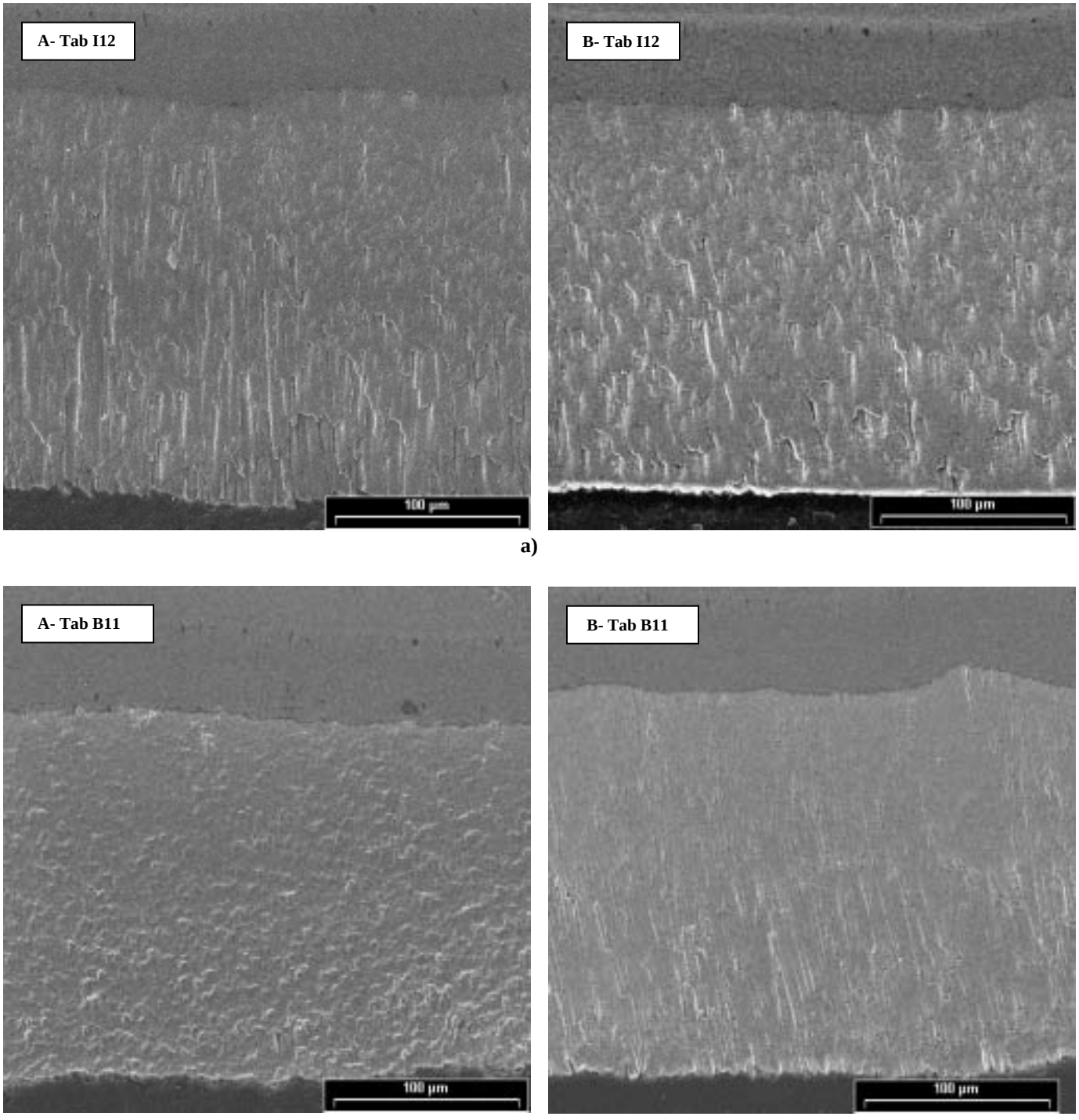

Figure 7: SEM Tab Cross-Sections of Surfaces A and B for Tabs I12 and B11

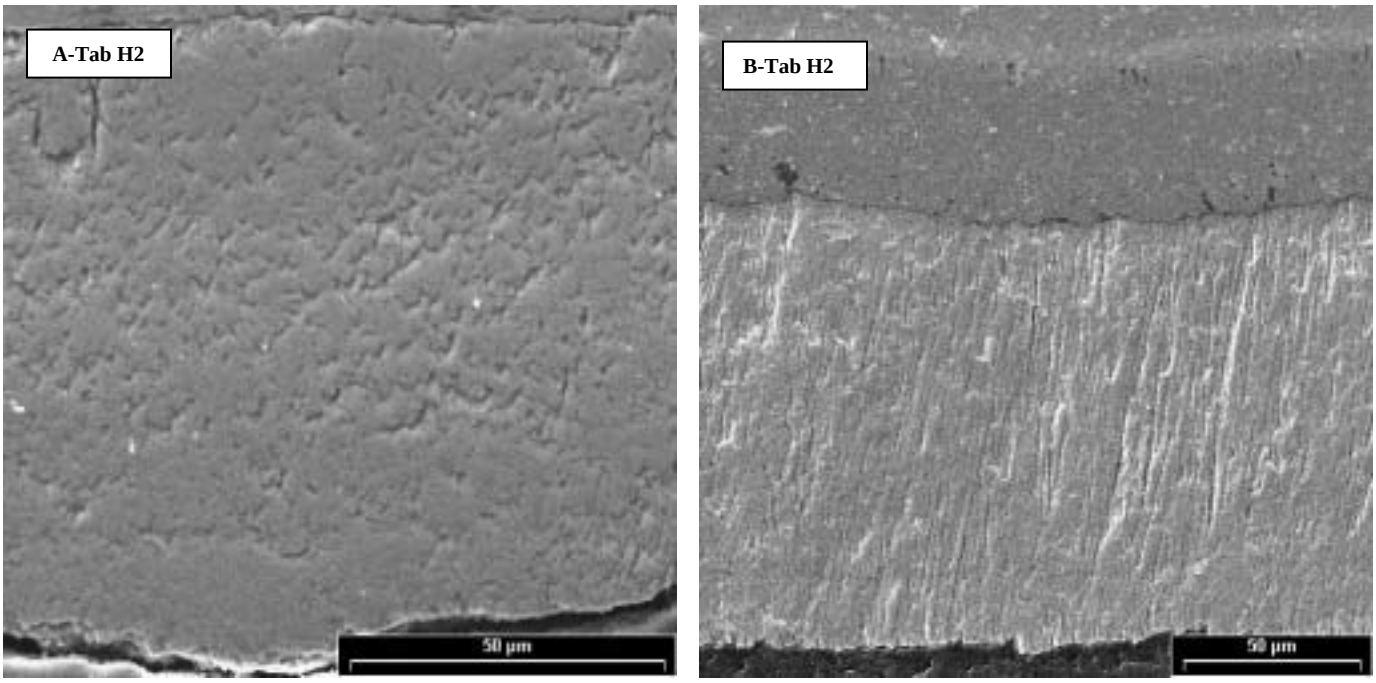

a)

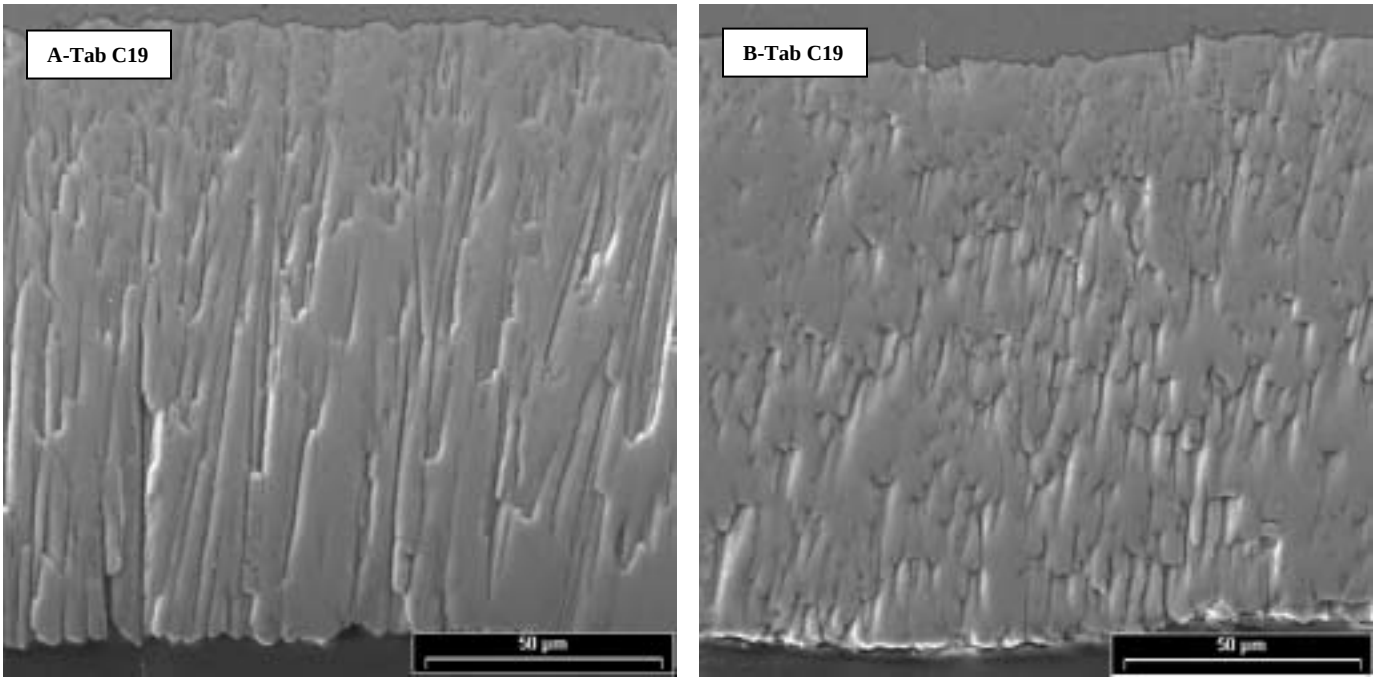

b)

Figure 8: SEM Tab Cross Sections of Surfaces A and B for Tabs H2 and C19

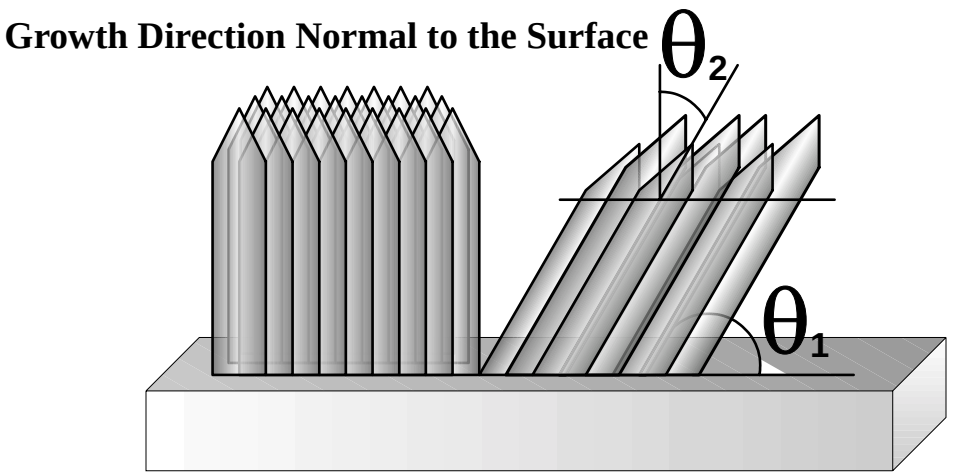

θ_1: Measured Column Growth Angle (CGA)

θ_2: Pole Figure Analysis Angle from Pole Figure Data

Figure 9: Angle Identification

Table 1: Angle Definitions and How They Were Determined

Name	Definition	Determined
VIA	Angle between the surface substrate and the direction of the vapor beam from the center of the closest ingot.	Coating Fixture Geometry and Tab Location and Height within the Coating Chamber
CGA	Angle at which the TBC column grows towards the closest ingot with respect to the surface substrate.	Cross-Sectional Microscopy
VIA Rotation	Number of degrees the VIA is rotated from the tab's x-axis (Figure 3) in order to point towards the closest vapor source.	Coating Fixture Geometry and Tab Location and Height within the Coating Chamber
CGA Rotation	Number of degrees the CGA is rotated from the tab's x-axis (Figure 3) in order to point towards the closest vapor source.	Cross-Sectional Microscopy
Inclination Angle	90 - the tilt angle from the pole figure. Tilt angle is defined as the number of degrees the given hkl plane is shifted from the center of the pole figure.	Pole Figure Analysis (90-θ_2 in Figure 9)
Rotation of Inclination Angle	Number of degrees the inclination angle is rotated in order to meet the pole figures closest x-axis.	Pole Figure Analysis

Table 2: Column Growth Angle and Vapor Incidence Angle (VIA) Information
(Figure 9 illustrates Angle Information)

Tab	VIA w/ Respect to Closest Ingot and Surface Normal	Angle of Rotation of the VIA (from tabs x-axis)	Column Growth Angle (CGA) Measurements A Surface B		Calculated Column Growth Angle (CGA) *(From A&B Surfaces)*	Angle of Rotation of the CGA (from tabs x-axis)
F6	***90°***	ingot1	88°	89°	***88°***	64° ingot 1
E7	***84°***	24° ingot 1	84°	79°	***78°***	62° ingot 1
I12	***60° (between ingots)***	41° ingot 2	87°	85°	***84°***	59° ingot 2
B11	***57° (between ingots)***	36° ingot 1or 2	N/A	78°	**Could not be**	**determined**
H2	***63°***	33° ingot 1	74°	76°	***69°***	41° ingot1
C19	***66°***	40° ingot 2	82°	77°	***75°***	59° ingot 2

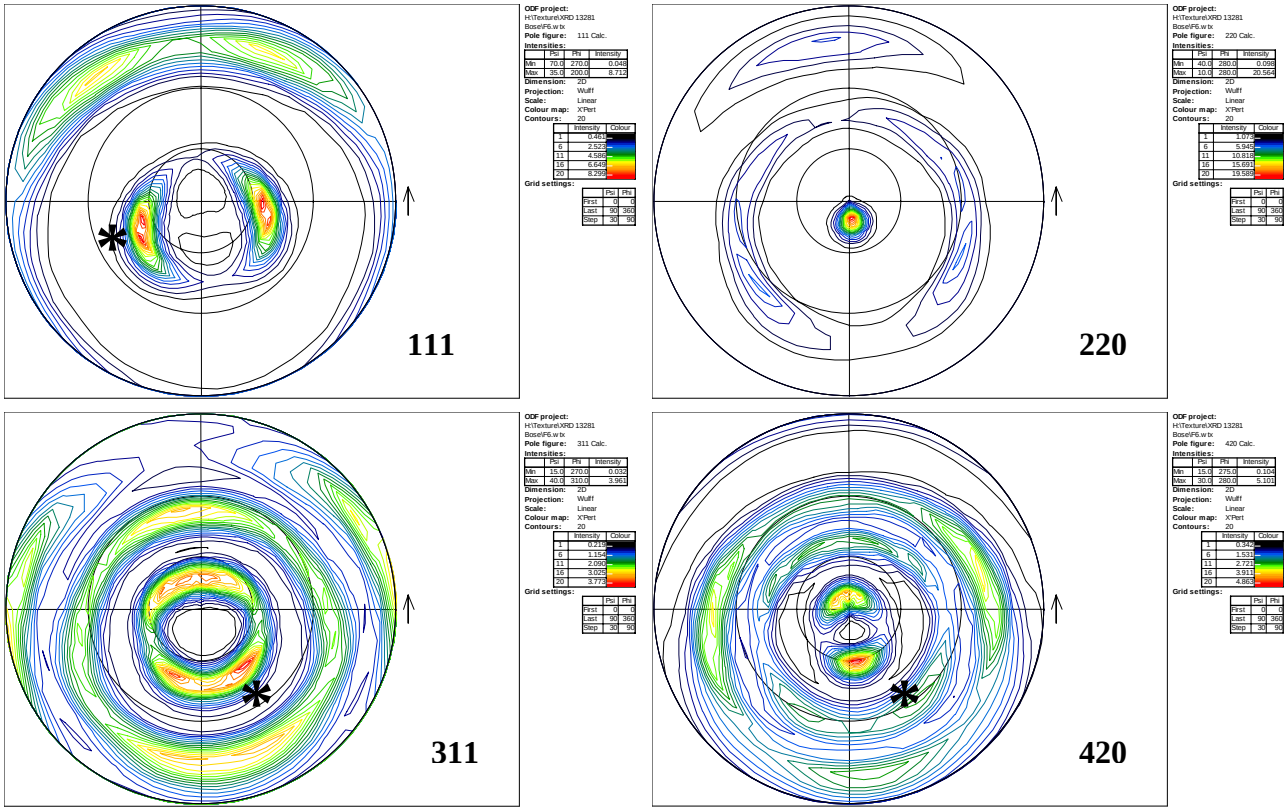

Figure 10: Pole Figures for Tab F6.

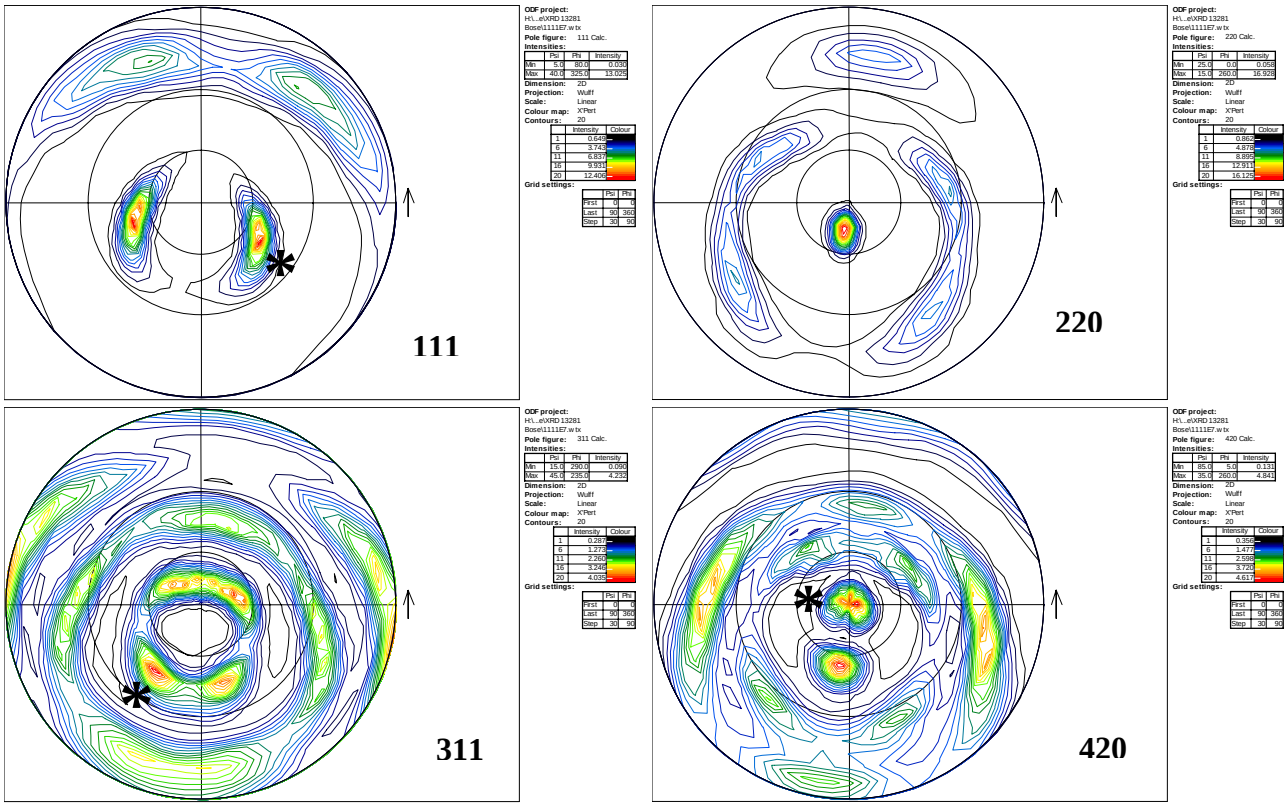

Figure 11: Pole Figures for Tab E7.

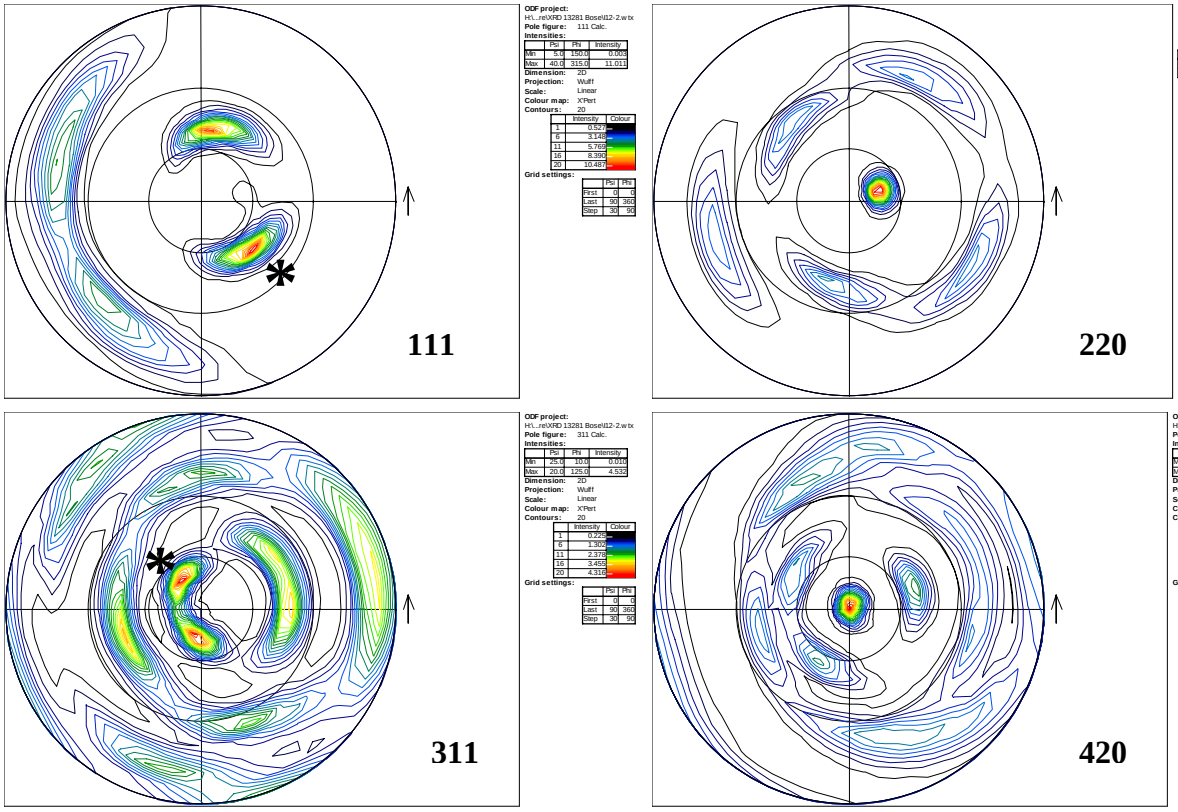

Figure 12: Pole Figures for Tab I12

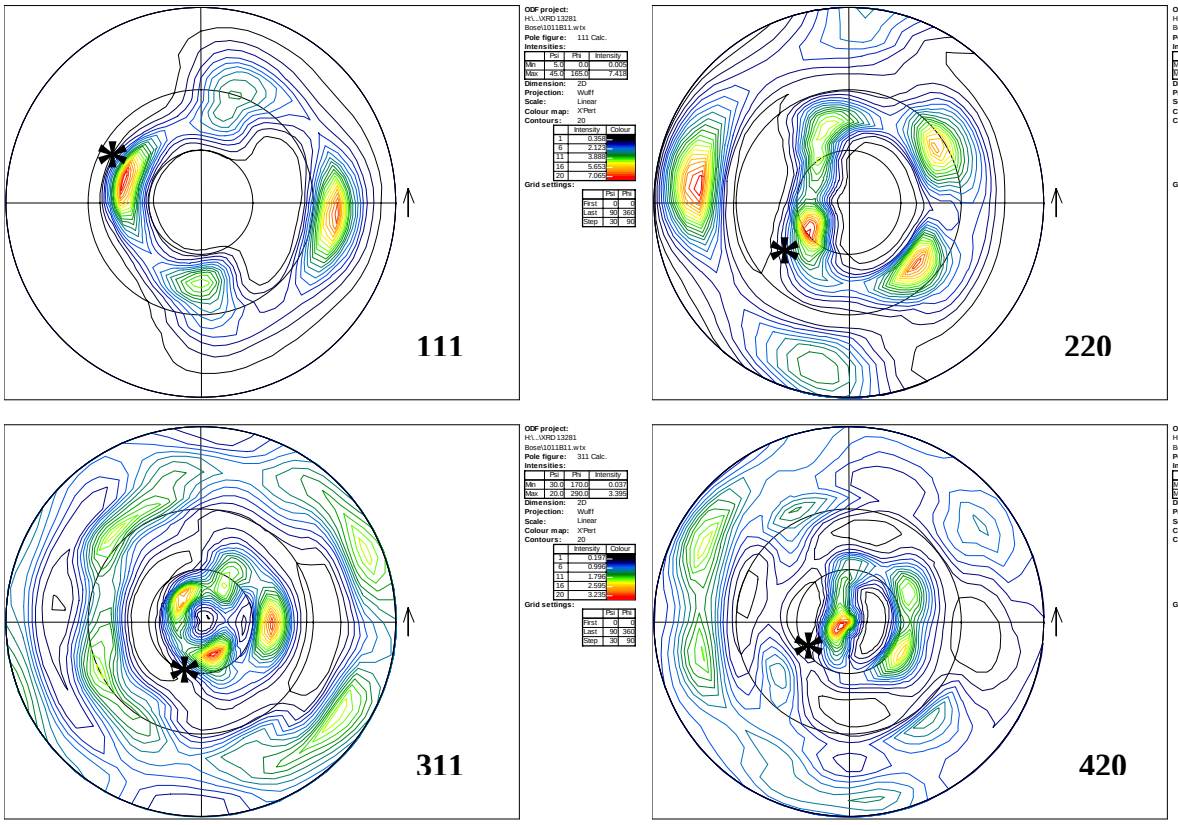

Figure 13: Pole Figures for Tab B11

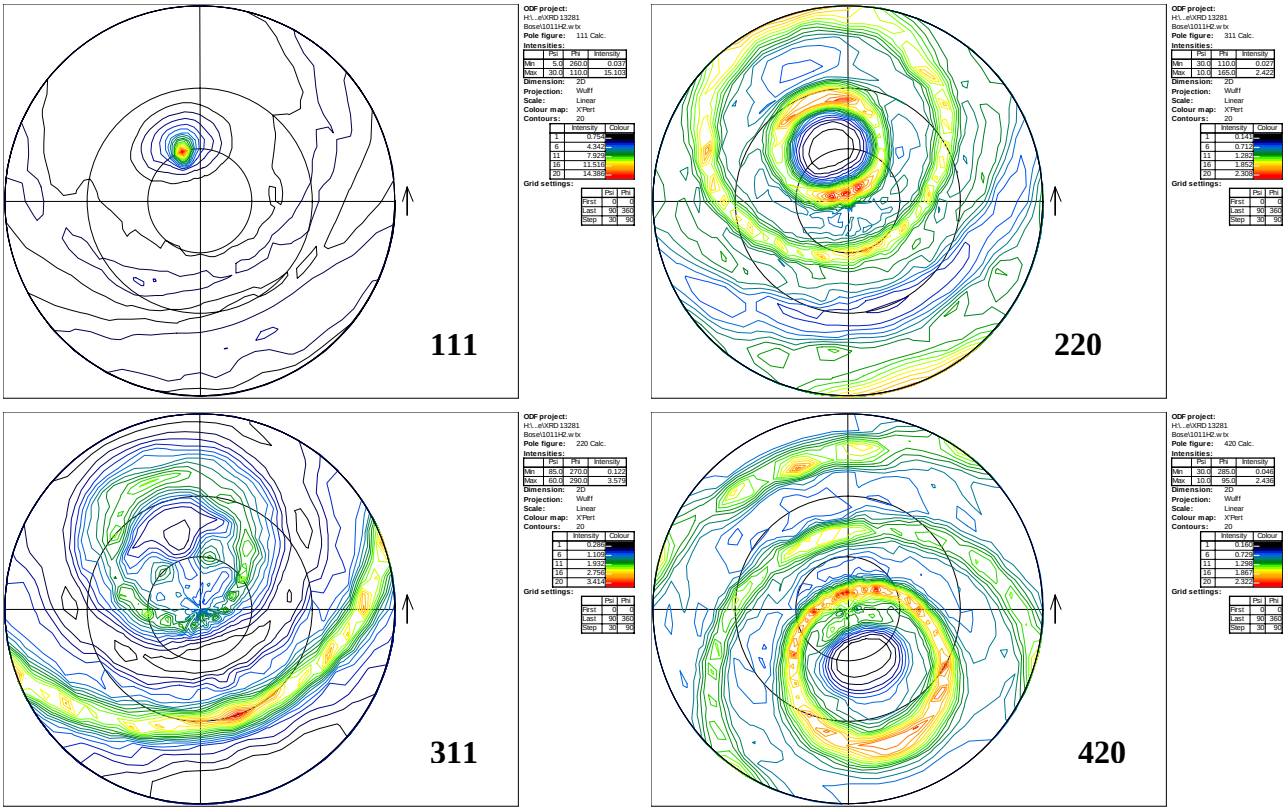

Figure 14: Pole Figures for Tab H2

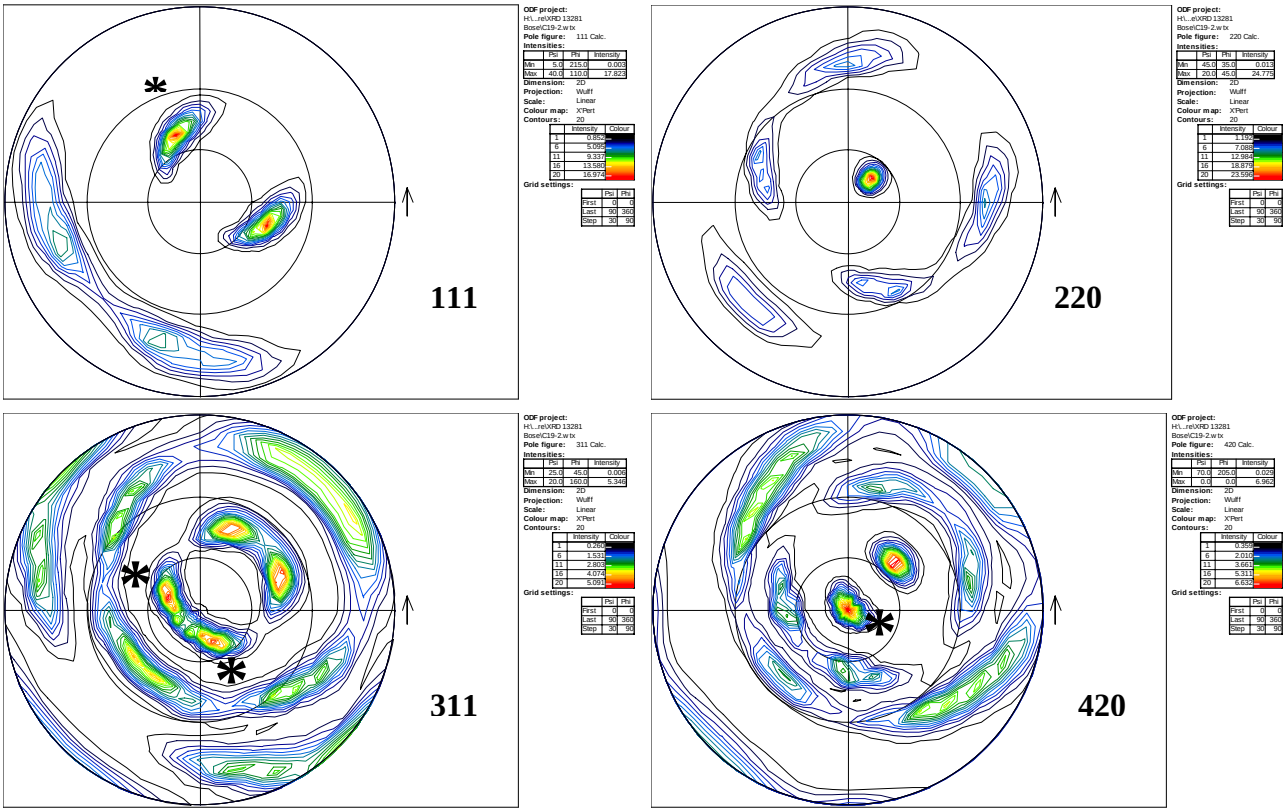

Figure 15: Pole Figures for Tab C19

Table 3: Pole Figure Analysis Data

Tab	hkl	Inclination Angle from Substrate Surface (90-θ_2)	Pole Figures Rotation Angle(closest x-axis)	Pole Figures General Growth Direction
F6	111	53°	24°	crystal growth points in the general direction of ingot 1 in both highlighted cases
	220	**79°**	**81°**	
	311	50°	68°	
	420	80°	80°	
E7	111	50°	35°	crystal growth points in the general direction of ingot 1
	220	**73°**	**80°**	
	311	45°	55°	
	420	0°	0°	
I12	111	50°	84°	crystal growth points in the general direction of ingot 2
	220	73°	20°	
	311	70°	56°	
	420	90°	0°	
B11	111	20°	5°	crystal growth points in the general direction of ingot 2
	220	**62°**	**35°**	
	311	70°	31°	crystal growth points in the general direction of ingot 1
	420	85°	26°	
H2	**111-fiber**	**60°**	**70°**	crystal growth general points towards ingot 1
C19	111	50°	60°	crystal growth points away from both vapor sources
	220	**70°**	**56°**	
	311	70°	11°	crystal growth general points towards ingot 2
	311	70°	58°	
	420	53°	55°	

Table 4: Determination of the Primary Growth Plane Based off VIA, CGA, and Pole Figure Data

Tab	VIA w/ Respect to Closest Ingot and Surface Normal	Angle of Rotation (VIA) (From tabs x-axis)	Column Growth Angle (CGA)	Angle of Rotation (CGA) (From Tabs x-axis)	Pole Figure Angle from Tabs Surface ($90-\theta_2$)	Pole Figure Rotation Angle (x-axis)	Primary Growth Plane Which Points Towards a Vapor Source
F6	***90°***	none	***88°***	64°	***79°***	81°	***<220>***
E7	***84°***	24°	***78°***	62°	***73°***	80°	***<220>***
I12	***60°***	41°	***84°***	59°	***70°***	56°	***<311>***
B11	***57°***	36°			***70°***	31°	
H2	***63°***	33°	***69°***	41°	***60°***	70°	***<111>fiber***
C19	***67°***	40°	***75°***	59°	***70°***	58°	***<311>***

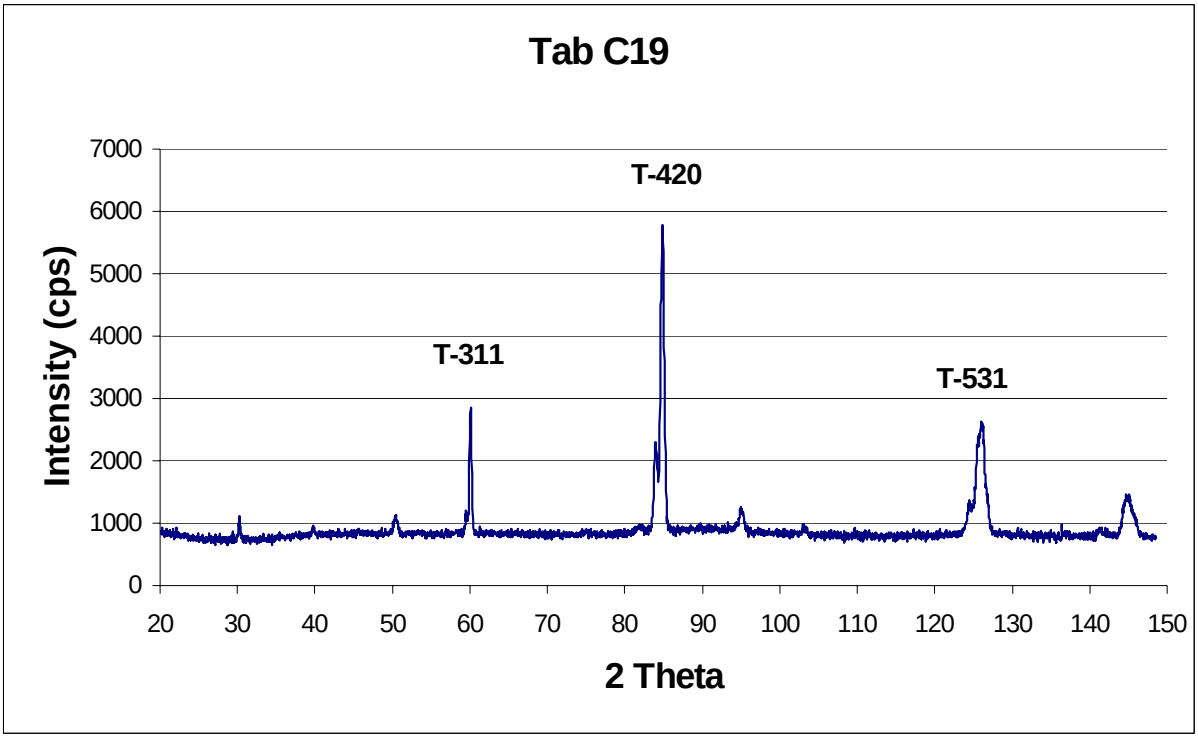

Figure 16: X-ray diffraction pattern of specimen C19.

Table 5: Planes of Greatest Normalized Intensity from XRD Patterns

Tab Location	Plane	Intensity
F6	*T-220*	*100%*
E7	T-220 T-420 T-531 T-111	100% 52% 39% 37%
I12	T-420 T-311	100% 40%
B11	T-620 T-420 T-200 T-311 T-511	100% 49% 48% 46% 38%
H2-	T-220 T-311 T-111	100% 99% 36%
C19	T-420 T-311 T-531	100% 39% 35%
ZrO_2 Powder Pattern (JCPDS Card # 17-923)	T-111 T-202 T-311	100% 65% 45%

Chapter IV

4.0 Summary

From the articles presented in this thesis, it has been found that microstructure and crystallographic texture are dependent on position in the EB-PVD coating chamber. The microstructure for coatings deposited on cylinders was shown to be a function of shadowing effects. A dense coating were found to be deposited on the bottom of the cylinder, but as the cylindrical position changed porosity developed and density decreased. The porosity increase was due to self-shadowing effects caused by surface curvature changes on the cylinder. Coating is first deposited on the bottom of the cylinder because EB-PVD is a "line of sight" process. As more coating is deposited on the bottom of the cylinder, the adjacent area is shadowed, causing an increase in porosity with position change.

The crystallographic texture differences for coatings deposited on cylindrical surfaces are attributed to the change in the vapor incidence angle. As surface curvature is increased (i.e. position changes from the bottom of the cylinder), the angle at which the depositing vapor hits the surface changes. Literature has shown that changes in vapor incidence angle leads to changes in crystallographic texture. Therefore, with the vapor incidence angle changing with surface curvature, crystallographic texture would change with surface curvature as was shown.

The microstructure and crystallographic texture of coatings deposited on flat plates was shown to be a function of the vapor incidence angle and substrate temperature. Depending on tab location the vapor incidence angle and substrate temperature change. For tabs located directly above the ingot, the substrate temperature is the hottest and the vapor incidence angle is 90 degrees(i.e. columns are growing normal to the substrate).

The higher the substrate temperature the more surface and volume diffusion occurs in the deposited coating, creating a certain microstructure and crystallographic texture. As the tab location varies, substrate temperatures and vapor incidence angles change (i.e. lower substrate temperature and lower vapor incidence angle), causing different microstructures and crystallographic textures to develop due to growth kinetics.

The current model for predicting TBC thickness deposited onto stationary cylinders must take into consideration other variables not accounted for in the model. This conclusion was drawn from the fact that in each experiment there was no exact (y=x) correlation for experimental thickness and predicted thickness. A compilation of all the cylinder experiments yielded a slope of the line less than 1 **(y= .81x),** which indicated others factors influence the deposition rate. The new thickness prediction model takes into consideration those other variables, which are believed to be the sticking coefficient and ricochet effect. The new model takes into consideration the slope of all the complied cylinder experiments (.81x) and uses that as the basis to represent the sticking coefficient and ricochet variables. The new model states:

$$d = 0.81\left[\frac{M_e}{\rho_{coating}}\left(\frac{\cos\theta\cdot\cos\phi}{\pi\cdot r^2}\right)\right]$$

Chapter V

5. Recommendations

I would recommend that future work be done to study the deposition rate, density, microstructure and crystallographic texture of TBCs deposited on rotated and stationary turbine blades. Turbine blades have a unique geometric shape, which would influence the deposition rate, density, microstructure, and crystallographic texture. Studying a turbine blade is more practical than a cylinder or a flat plate, but you must understand the basic geometric shapes as was explained in this thesis. I would also recommend varying process parameters such as height, rotation rate, and substrate surface temperature to determine how the TBC microstructure and texture are affected on a turbine blade. Knowing how crystallographic texture, microstructure, density and deposition rate are affected by the process parameters will allow for control of the mechanical and thermal properties of the depositing TBC on a turbine blade.

I would also recommend that the mechanical and thermal properties be experimental determined for various crystallographic textures of TBCs deposited on flat plates. This would allow for determination of what crystallographic texture plane should try to be deposited on turbine blades in order to get the best possible mechanical and thermal properties.

I would also recommend that the substrate material be dissolved off so the TBC itself remains as one piece. With the remaining TBC coating, look at the microstructure and texture on the backside of the coating. This would allow comparison between back and front side of the coating to see if what differences there are in microstructure and crystallographic texture.